Elsevier Editorial System(tm) for Geochimica et Cosmochimica Acta
Manuscript Draft

Manuscript Number: W7940R3

Title: (W7940)Bacterial dissolution of fluorapatite as a possible source of elevated dissolved phosphate in the environment

Article Type: Article

Corresponding Author: Dr. Mu-hua Feng,

Corresponding Author's Institution: Chinese Academy of Sciences

First Author: Mu-hua Feng

Order of Authors: Mu-hua Feng; Bryne T Ngwenya; Lin Wang; Wenchao Li; Valerie Olive; Robert M Ellam

Abstract: In order to understand the contribution of geogenic phosphorus to lake eutrophication, we have investigated the rate and extent of fluorapatite dissolution in the presence of two common soil bacteria (Pantoea agglomerans and Bacillus megaterium) at T = 25 °C for 26 days. The release of calcium (Ca), phosphorus (P), and rare earth elements (REE) under biotic and abiotic conditions was compared to investigate the effect of microorganism on apatite dissolution. The release of Ca and P was enhanced under the influence of bacteria. Apatite dissolution rates obtained from solution Ca concentration in the biotic reactors increased above error compared with abiotic controls. Chemical analysis of biomass showed that bacteria scavenged Ca, P, and REE during their growth, which lowered their fluid concentrations, leading to apparent lower release rates. The temporal evolution of pH in the reactors reflected the balance of apatite weathering, solution reactions, bacterial metabolism, and potentially secondary precipitation, which was implied in the variety of REE patterns in the biotic and abiotic reactors. Light rare earth elements (LREE) were preferentially adsorbed to cell surfaces, whereas heavy rare earth elements (HREE) were retained in the fluid phase. Decoupling of LREE and HREE could possibly be due to preferential release of HREE from apatite or selective secondary precipitation of LREE enriched phosphates, especially in the presence of bacteria. When corrected for intracellular concentrations, both biotic reactors showed high P and REE release compared with the abiotic control. We speculate that lack of this correction explains the conflicting findings about the role of bacteria in mineral weathering rates. The observation that bacteria enhance the release rate of P and REE from apatite could account for some of the phosphorus burden and metal pollution in aquatic environments.

Bacterial dissolution of fluorapatite as a possible source of elevated dissolved phosphate in the environment

Mu-hua Feng[a], Bryne T. Ngwenya[b], Lin Wang[c], Wenchao Li[a], Valerie Olive[d] and Robert M. Ellam[d].

[a] State Key Laboratory of Lake Science and Environment,

Nanjing Institute of Geography & Limnology,

Chinese Academy of Sciences,

73 East Beijing Road, Nanjing 210008, P.R. China.

[b] Microbial Geochemistry Laboratory,

School of GeoSciences,

University of Edinburgh,

West Mains Road, Edinburgh EH9 3JW, UK.

[c] Chemistry and Environmental Science Department ,

Yuxi Normal University,

Yuxi, 653100, P.R. China.

[d] Scottish Universities Environmental Research Centre,

Rankine Avenue,

East Kilbride, G75 0QF, UK.

Abstract

In order to understand the contribution of geogenic phosphorus to lake eutrophication, we have investigated the rate and extent of fluorapatite dissolution in the presence of two common soil bacteria (*Pantoea agglomerans* and *Bacillus megaterium*) at T = 25 °C for 26 days. The release of calcium (Ca), phosphorus (P), and rare earth elements (REE) under biotic and abiotic conditions was compared to investigate the effect of microorganism on apatite dissolution. The release of Ca and P was enhanced under the influence of bacteria. Apatite dissolution rates obtained from solution Ca concentration in the biotic reactors increased above error compared with abiotic controls. Chemical analysis of biomass showed that bacteria scavenged Ca, P, and REE during their growth, which lowered their fluid concentrations, leading to apparent lower release rates. The temporal evolution of pH in the reactors reflected the balance of apatite weathering, solution reactions, bacterial metabolism, and potentially secondary precipitation, which was implied in the variety of REE patterns in the biotic and abiotic reactors. Light rare earth elements (LREE) were preferentially adsorbed to cell surfaces, whereas heavy rare earth elements (HREE) were retained in the fluid phase. Decoupling of LREE and HREE could possibly be due to preferential release of HREE from apatite or selective secondary precipitation of LREE enriched phosphates, especially in the presence of bacteria. When corrected for intracellular concentrations, both biotic reactors showed high P and REE release compared with the abiotic control. We speculate that lack of this correction explains the conflicting findings about the role of bacteria in mineral weathering rates. The observation that bacteria enhance the release rates of P and REE from apatite could account for some of the phosphorus burden and metal pollution in aquatic environments.

1. INTRODUCTION

We present experimental data on the rate and extent of fluorapatite dissolution in the presence of two common soil bacteria in an attempt to investigate whether microbial dissolution of this mineral in phosphate mine wastes and other environmental systems could contribute to phosphate and trace metal pollution of freshwaters. The motivation for our study is the observation of a possible temporal link between phosphate mining and eutrophication of Lake Fuxianhu in Yunnan Province in China. The period since phosphate mining commenced in the lake watershed in 1980 is associated with a progressive increase in phytoplankton abundance (Li et al., 2007). Rivers draining the mined land have elevated P concentrations and sampling of the lake water where these rivers drain into the lake also shows elevated concentrations relative to areas fed by pristine rivers (Feng et al., 2008).

Most of the loading of phosphorus to freshwater is considered to be due to agricultural, industrial, and domestic sewage inputs (Ng Kee Kwong et al., 2002; Salvia-Castellví et al., 2005). As a result, relatively few studies have examined phosphorus loading from natural phosphate-containing rocks or mined waste rock. This lack of consideration of natural and mined phosphate as a source of phosphorus for eutrophication is understandable given the low solubility of phosphate minerals, in particular apatite, under natural (circum-neutral) pH conditions. For example, Köhler et al. (2005) showed that apatite dissolution rates decrease by about 3 orders of magnitude between pH 5 and pH 8. Similarly, Chaïrat et al. (2007) have shown that apatite dissolution rates decrease between pH 3 and pH 7 but are independent of pH between pH 7 and pH 10. Nevertheless, weathering and erosion of catchment rocks has been recognised as an important source of phosphate-induced eutrophication of

freshwaters as far back as the early 1970s (e.g. Golterman, 1973).

Given that most phosphate mines are located near freshwater lakes in China, as shown by the Lake Fuxianhu example and that mined waste rock can often generate acidic mine waters, we predict that extensive mining without pollution control and restoration of phosphate mined lands is likely to be a significant cause of the phosphorous burden of watersheds. We hypothesise further that micro-organisms are likely to be a major factor in the release of this phosphorus. This is based on a wealth of literature from the field of botany/agriculture which documents a range of bacteria and/or fungi living in symbiotic relationships with plants, for which they help to solubilise phosphate minerals (Harris et al., 2006; Kang et al., 2009). Apparently, these microcosms achieve phosphate solubilisation by decreasing the pH of the growth medium and/or microcosms (Welch et al., 2002; Chatli et al., 2008; Kang et al., 2009). Interestingly for this study, there are indications that laboratory experiments are good predictors of the phosphate-solubilising potential of micro-organisms (Harris et al., 2006).

Microbial dissolution of apatite is also of significance in relation to the mobility and bioavailability of trace metals. The structure of apatite accommodates relatively high abundances of many trace elements (including rare-earth elements (REE), Sr, Y, Mn, Th and U), which are likely to be released upon apatite dissolution, but there is little quantitative data to characterize the migration of trace elements associated with apatite during microbial dissolution. A field-based study by Taunton et al. (2000) showed that micro-organisms can take up some of the elements released by dissolving apatite, in addition to precipitation of secondary REE phosphates such as rhabdophane and florencite, providing a mechanism for immobilizing the metals. Experiments by Köhler et al. (2005) showed that apatite dissolution also resulted in fixation of the

REE into the secondary mineral rhabdophane, and fractionation of the REE due to preferential fixation of the LREE by this mineral.

The aim of this study was to determine the role of microbes in the supply of soluble phosphorus to the environment, with potential for widespread eutrophication. Specific objectives were (i) to determine the dissolution kinetics of apatite in the presence of microbes, and (ii) to develop a mechanistic understanding of the role of this process on the supply of soluble phosphorus and the mobility of apatite-hosted trace elements, particularly lanthanides.

2. MATERIAL AND METHODS

2.1. Fluorapatite seed preparation and characteristics

Since the main phosphate mineral in the mine and waste rock piles in Fuxianhu Watershed is fluorapatite, Durango fluorapatite (FAP) was chosen as a representative because it is well known and has been well characterised for its major chemistry and trace metal concentrations (Young et al., 1969). High purity Durango fluorapatite was kindly supplied by Dr. A.N. Mariano. The FAP sample was crushed by hand and sieved to collect the 150-500 μm size fractions for the dissolution experiments. The particle grains were ultrasonically cleaned, first in de-ionized water, and then in acetone, by separating the ultra fine suspension at the end of each cleaning cycle, which lasted for 10 min. Four to seven water cycles and five to nine acetone cycles were conducted to remove fine particles. The fluorapatite samples were then dried at 60 °C overnight. The purity of the sample was guaranteed by removing impure grains under a binocular microscope. No fines were observed when the cleaned apatite grains

were subsequently analysed by SEM. The surface area of the cleaned apatite was 0.0038 m^2/g as determined by BET-N_2 method (ASAP 2020M, Micromeritics Inc., USA) at the Department of Chemistry, University of Nanjing. Concentrations of major elements and REE in the apatite were determined by ICP-OES and ICP-MS after digestion in 3 ml of $HNO_3/HClO_4/HF$ mixture in PTFE vessels under high-pressure conditions (Zhang and Shan, 1997). Repeated analysis of geochemical standard reference samples GSD-9 and GSD-11 (Xie et al., 1989) yielded external reproducibility better than 5%. Arsenic concentrations were determined by hydride generation atomic fluorescence spectrometry (HG-AFS). Concentrations of major anion elements (F, Cl) were determined by ion selective methods after digestion in 3 ml 16.75 mol/L NaOH solution. Chemical analysis of the apatite is listed in Table 1.

2.2. Biomass choice and preparation

The experiments were conduced using two types of bacteria, *Pantoea agglomerans* and *Bacillus megaterium*. *Pantoea agglomerans* is a common soil organism, often associated with plant roots and belongs to *Enterobacteriacea*, a group of bacteria that have been shown to solubilise rock phosphate (Zhao et al., 2002). We used a Cu-resistant, gram-negative strain which has been well characterised for its cell surface and metal adsorption properties (Ngwenya et al., 2003; Ngwenya, 2007; Ngwenya et al., 2009). The strain of *B. megaterium* is a common gram-positive, rod-shaped endospore-forming bacterium available from the National Collection of Industrial, Food and Marine Bacteria (NCIMB 8508). This strain was chosen as a reference because a previous study had shown its ability to increase the rate of dissolution of mineral-bound phosphate (Hutchens et al., 2006). These two types of

bacteria had different cell size and metabolic behavior and were compared in the present study.

The bacteria were grown for 15 h in 2 L flasks containing 1 L nutrient broth media to obtain bacteria in the exponential phase of growth, and then were harvested by centrifugation for 20 min at 23,420 g and 4 °C. The cells were resuspended in 20 mL of sterile (autoclaved) MilliQ water and vortexed for about 20 min. This process was repeated three times. The resulting cell pellet was resuspended in 10 mL of a minimal medium containing 0.012 g/L KBr, 0.2 g/L glucose, and 0.38 g/L NH_4Cl. The solution was adjusted to pH 7 with dilute HCl or NH_4OH and then sterilized. The final pH of the minimal medium was 6.2 ± 0.05. A preliminary test suggested that the minimal medium combined with fluorapatite could support microbial metabolism for more than 30 days. Here the fluorapatite was supplied as the P source, so the extra dissolved P wasn't added to the medium. The minimal medium was used in the following dissolution experiments. All of the above procedures were conducted under sterile conditions to prevent microbial contamination.

2.3. Batch dissolution experiments

Dissolution experiments were conducted in sterile 500 mL Corning polycarbonate Erlenmeyer culture flasks with vented caps (0.22 μm PTFE membranes) containing 400 ml of the minimal medium as described above. There were two sets of experiments involving viable bacteria and fluorapatite: fluorapatite with *B. megaterium* (FAP + Bm), and fluorapatite with *P. agglomerans* (FAP + Pa). Abiotic controls with fluorapatite (FAP) were conducted to check the dissolution effect of reactive solution on apatite. For both biotic and abiotic experiments with fluorapatite,

151 the 2.4 g fluorapatite particles were sterilized by autoclaving for 1 h and then
152 introduced into the culture flasks. The biotic experiments with *B. megaterium* and *P.*
153 *agglomerans* were inoculated with 100 μL of the washed cultures. Conventional plate
154 counting techniques showed that the reactors with *B. megaterium* and *P. agglomerans*
155 had initial cell densities of ~10^5 and 10^7 CFU (colony forming units)/mL immediately
156 after inoculation, respectively. Each experiment was performed in triplicate. The
157 suspensions were allowed to equilibrate on a shaker incubator maintained at 25 ± 1 °C
158 for up to 26 days.
159 During the dissolution experiments, aliquots (6 mL) were removed with sterile
160 serological pipettes daily for chemical analysis for the first 7 d, and then every 3 d for
161 the rest of the experiment. Each 6-mL aliquot was immediately processed as follows:
162 100 μL was unfiltered for plate counting, 4 mL was filtered with a 0.22 μm PES
163 Membrane (Millex 33 mm) for released ions measurements, and the remaining ~2 ml
164 solution was unfiltered for pH analysis. The 4-mL filtered aliquot was acidified to 2%
165 v/v HNO_3 and stored at 4 °C before ionic analysis. The sampling process was
166 conducted under sterile conditions and during the entire period, we did not detect any
167 microbial contamination. Additional controls containing cells but no apatite (Bm and
168 Pa) were also set to investigate the bacterial behavior in the minimal medium without
169 apatite, in which 0.0056 g/L KH_2PO_4 was added to support bacterial metabolism.
170

171 **2.4. Biomass collection**

172

173 Upon completion of dissolution experiments, the remaining fluids (~240 mL) of biotic
174 reactors were collected to measure intracellular elemental concentrations. The liquid
175 samples were weighed and centrifuged at 23,420 g for 20 min. The cell pellet was

washed with MilliQ water three times and dried at T = 60 °C. The dried biomass was completely digested in concentrated ultrapure HNO_3, dried, and redissolved in ultrapure 2% HNO_3. The resulting solutions were passed through 0.22 μm PES membrane filter, and diluted to 20 mL by ultrapure 2% HNO_3.

2.5. Chemical analysis and data treatment

For Ca, P and K analysis, the acidified solutions were analysed directly by ICP-OES (Perkin ELmer Optima 5300, Perkin Elmer Inc, USA) at the University of Edinburgh using matrix-matched standards. The accuracy of the procedure was measured by including a certified (M6) standard diluted to bring the concentrations to within the range of our samples. The precision was better than 2% across the whole range of concentrations analysed.

For rare earth elements (REE) analysis, the sample solutions were diluted 5 fold with ultrapure 5% HNO_3 and metal concentration was determined using an Agilent 7500 + Quadrupole mass spectrometer at the Scottish Universites Environmental Research Centre (SUERC). The following REE isotopes were chosen to minimize isobaric interferences: ^{139}La, ^{140}Ce, ^{141}Pr, ^{145}Nd, and ^{146}Nd (mean value), ^{147}Sm, and ^{149}Sm (mean value), ^{151}Eu, and ^{153}Eu (mean value), ^{157}Gd, ^{159}Tb, ^{163}Dy, ^{165}Ho, ^{166}Er, ^{169}Tm, ^{172}Yb, and ^{175}Lu. Indium, Rhenium, and Ruthenium were selected as internal standards to monitor the condition of the VG PQ II+ within each session. The accuracy of the procedure was measured by including an international environmental reference material BCR-1 (Govindaraju, 1984). The precision was better than 3% for all REE across the whole measured procedure.

Species distribution, mineral saturation indices and ion-activity were calculated using

Visual Minteq 3.0. Due to batch reactors being partially open to the atmosphere, atmospheric CO_2 pressure was fixed as 380 μatm. The average solution concentrations of Ca, P, F, and REE were used as input.

3. Result and discussion

3.1. Cell growth during apatite dissolution

Figure 1 shows recorded cell growth during dissolution experiments for cultures with and without apatite. Assuming phosphate supply to be limiting, we expected to see no growth in control flasks containing no apatite and this is confirmed by cultures of *B. megaterium*, where cell densities decreased from the initial ~10^5 CFU/mL to less than ~30 CFU/mL after three days. Cell densities of *B. megaterium* in the reactors with apatite declined from the initial densities of ~10^5 CFU/mL to ~10^4 CFU/mL in the first day and then increased to ~10^5 CFU/mL for the rest of the experiment. These data demonstrate that *B. megaterium* requires phosphorus for growth, which it acquires by solubilising apatite in the absence of dissolved phosphate. By contrast, both reactors with and without apatite showed an increase in cell densities of *P. agglomerans* from ~10^7 CFU/mL to ~10^8 CFU/mL two days after inoculation and then remained more or less constant afterward, with higher cell counts in the apatite-amended cultures. A large number of micro-organisms accumulate and store excess phosphorus in the form of polyphosphates, which they can use as an internal resource when the external concentration of phosphorus is limiting (Kuhl, 1974; Powell et al., 2009; Hamdali et al., 2010). Apparently, *P. agglomerans* demonstrates this trait and can use phosphate accumulated from the media during growth of the

innoculum in nutrient broth.

3.2. Dissolved major element concentrations

The temporal evolution of aqueous Ca, P and pH during the dissolution experiments is illustrated in Fig. 2. The concentration data (Ca and P) were corrected for the decrease in fluid volume and loss of elemental mass during sampling according to the method of Wu et al. (2007). The aqueous concentration of Ca and P as a function of time showed similar patterns in both biotic and abiotic reactors. The solution Ca and P concentration increased rapidly during the first day of the experiment and then increased more gently with time. The attainment of steady state concentration was estimated to be the time when the slope of the concentration-time curve approaches zero, implying that the rate of breakdown of the leached surface is equal to the diffusion rate (Lasaga, 1984). In this regard, we used Ca concentrations to determine steady state attainment, since P data did not achieve steady-state for biotic reactors. The concentration of Ca reached steady state after 6 days in the reactors with *P. agglomerans* and apatite, and after 9 days for the reactors with *B. megaterium* and apatite, while the Ca and P concentration became constant after 16 days in the cell-free control. Thus the presence of bacteria accelerated attainment of steady state relative to controls. Furthermore the biotic reactors yielded significantly higher solution Ca and P concentrations than the abiotic reactors, particularly in the early days, although the final steady state value for the abiotic reactors was identical to the biotic *B. megaterium* value for Ca (Fig. 2a). Clearly and based on Ca, it appears that the initial dissolution rate of fluorapatite is marginally higher in the presence of bacteria.

Following an initial decrease in pH, there was concomitant increase in pH with aqueous Ca and P concentration in both biotic reactors. For the reactors with *P. agglomerans* and apatite, the pH initially decreased slightly from 6.2 to 6.0 and then increased to 6.6 by day 5. It also showed a modest decrease to 6.2 by day 16. The pH in the reactors with *B. megaterium* and apatite increased slowly to pH 6.2 by day 11, following a sharp decline from 6.2 to 5.8 in the first day. However, the increase in solution Ca and P concentration was accompanied by decrease of pH in the cell-free control (following an increase to 6.5 after 2 days). A similar phenomenon was observed in apatite dissolution experiments at acidic pH where the initial increase in pH was accounted for by ion exchange between mineral-bound Ca and hydrogen ion in solution (Guidry and Mackenzie, 2003), although the subsequent decrease in pH was not explained. In the present study, the pH decrease for the duration of experiment could partly be due to complexation between REE and phosphate and volatilization of ammonia, as discussed below.

There are several reactions in the biotic reactor that consume protons resulting in the increase of pH. The first is the acid dissolution of fluorapatite, which occurs by the following reaction:

$$Ca_{10}(PO_4)_6F_2 + 11H^+ \rightarrow 10Ca^{2+} + 5H_2PO_4^- + HPO_4^{2-} + 2F^- \quad (1)$$

This reaction is based on the fact that the molar distribution of aqueous inorganic species in solution as calculated by Visual Minteq 3.0 is dominated by $H_2PO_4^-$ and HPO_4^{2-}, constituting about 90% and 9.3% of total phosphate, respectively.

The second possibility is surface protonation of fluorapatite (Wu et al., 1991). Fluorapatite surfaces are thought to have two different types of surface groups,

276 $\equiv Ca\text{-}OH_2^+$ and $\equiv P\text{-}O^-$. Speciation of hydroxylated mineral surface groups is pH
277 dependent, which controls FAP dissolution rate (Guidry and Mackenzie 2003). It is
278 assumed that phosphate site protonation dominates within the pH range 5-7 for our
279 system:
280
281 $\equiv P\text{-}O^- + H^+ \Leftrightarrow \equiv P\text{-}OH$ (2)
282
283 Finally, ammonification of amino acids produced by lysing cells during cell death
284 phase could also lead to an increase in pH (Lee and Beveridge, 2001):
285
286 $R\text{-}CH(NH_2)\text{-}COOH + H_3O^+ \Leftrightarrow R\text{-}C(O)\text{-}COOH + NH_4^+ + H_2O$ (3)
287
288 As shown by growth curves in Fig. 1, CFU shows maintenance of a constant viable
289 population in the culture for up to 26 days of the experiment. Nevertheless,
290 examination of a sub-sample of the suspension using LIVE/DEAD viability staining
291 showed a significant proportion of the cells were dead, which could contribute to
292 ammonification.
293 Meanwhile, there are several reactions that produce protons and hence could explain
294 the lowering of pH. One of these is heterotrophic metabolism of the cells during cell
295 growth phase (Wu et al., 2007):
296
297 $11C_6H_{12}O_6 + 24O_2 + 8NH_4^+ + 8HCO_3^- \Leftrightarrow 8C_5H_8O_2N + 34CO_2 + 54H_2O$ (4)
298
299 where $C_5H_8O_2N$ is an assumed chemical formula for a pure culture of prokaryotic
300 cells. Another reaction is volatilization of NH_3:

$$NH_4^+ + H_2O \Leftrightarrow NH_3\uparrow + H_3O^+ \quad (5)$$

Furthermore, a recent study has shown that REE nanocrystals precipitate readily on surfaces of micro-organisms (yeast cells) in the presence of phosphate (Jiang et al., 2010). Given the high REE content of Durango apatite, the complexation and precipitation of REE phosphates is a possible mechanism for decreasing pH in our culture and abiotic experiments:

$$REE^{3+} + HPO_4^{2-} + nH_2O \Leftrightarrow REE(PO_4)\cdot nH_2O\downarrow + H^+ \quad (6)$$

$$REE^{3+} + H_2PO_4^- + nH_2O \Leftrightarrow REE(PO_4)\cdot nH_2O\downarrow + 2H^+ \quad (7)$$

Moreover, the flasks were partially open to the atmosphere using vented caps (0.22 μm PTFE membranes), hence the atmospheric CO_2 would take part in the complexation reaction of REE with carbonic acid, which could also lower pH in the reaction:

$$REE^{3+} + CO_2 + H_2O \Leftrightarrow REE(HCO_3)^{2+} + H^+ \quad (8)$$

For biotic reactors, heterotrophic metabolism of the cells produced respired CO_2 directly into the reactor solutions as indicated by Eq. (4). However, we didn't observe the sharp pH decrease that could be due to carbonic acid production in comparison to changes observed by Wu et al. (2007), who measured pH values of about 4.3 in similar systems in response to respiratory CO_2 acidification. Wu et al. (2008) also did not detect dissolved CO_2 and assumed that respired CO_2 had vented to the atmosphere.

The speciation calculated by Visual Minteq 3.0 showed that saturation indices for REE carbonate/hydrocarbonate complexes were negative (data not shown), which suggested that REE carbonate/hydrocarbonate complexes were far from equilibrium. Therefore, only a small amount of atmospheric CO_2 and respired CO_2 participated in complexation with REE contributing to pH decrease in the biotic reactors.

If we take the abiotic reactor as an example to explain the role of REE complexation in lowering pH, we note that the decrease in pH from 6.5 to 6.0 in the late stage of the experiment of the abiotic control yielded 6.8×10^{-7} mol/L H^+. The total molar concentration of REE in solution was about 1.5×10^{-7} mol/L. Hence, the interactions in Eqs. (6) - (8) accounted for the addition of 1.5×10^{-7} - 3.0×10^{-7} mol/L H^+. This shows that REE complexation can explain up to 50% of the pH decrease, with the rest being probably due to volatilization of NH_3.

The dissolved Ca:P ratios in biotic and abiotic reactors are shown in Fig. 2c. For biotic and abiotic reactors, the Ca:P ratios were very high for the first 4-5 days, decreased with time, but remained above the stoichiometric mineral ratios for the duration of the experimental run. One explanation proposed in previous work was the initial preferential release of Ca coupled to phosphate hydrolysis (Wu et al., 1991; Chaïrat et al., 2007), which resulted in the formation of a calcium-deficient leached surface phase (Valsami-Jones et al., 1998; Guidry and Mackenzie, 2003). The protonated Ca depleted apatite constitutes the precursor complex of apatite dissolution (Chaïrat et al., 2007). The solution Ca:P ratios in the reactors with *B. megaterium* and apatite showed close to stoichiometric ratios rather than those of *P. agglomerans* and the abiotic reactor. The complexation and precipitation of $REE(PO_4)$ (Eq. 6 above) could account for the non-stoichiometric dissolution and pH decrease in the cell-free reactors which was in agreement with the result of Köhler et al. (2005). It is also

possible that *P. agglomerans* is accumulating phosphorus in its cells, consistent with the inference from growth curves (Fig. 1 and section 3.1).

3.3. Dissolution rate

Apatite dissolution rates were computed from the change in concentration of Ca in solution over time normalized to fluorapatite surface area using the following linear rate law:

$$r = \frac{\partial C_{Ca}}{\partial t} \frac{M_{sol}}{\nu_{Ca} s} \quad (9)$$

where $\partial C_{Ca}/\partial t$ refers to the slope of the Ca concentration versus time in Fig. 2a, M_{sol} represents the mass of solution in the closed system reactor, ν_{Ca} refers to the stoichiometric number of moles of Ca in 1 mol of apatite, and *s* denotes the total mineral surface area present in the reactor.

The rates were calculated using data over the time interval of linear Ca release, excluding the first day during which nonlinear dissolution, possibly due to preferential dissolution of defects caused by the crushing process (Lasaga, 1984). Linear phases were 2 to 6 days for the reactors with *P. agglomerans*, 2 to 9 days for the reactors with *B. megaterium*, and 2 to 16 days for the abiotic control.

Results of dissolution rates generated from Eq. (9) are listed in Table 2. The dissolution rate at 25 °C and pH 6.2, in the absence of bacteria, was found to be 3.61 ± 0.10 × 10^{-15} mol/cm^2/s, which was close to that measured for the abiotic control by Hutchens et al. (2006) under similar experimental conditions. They determined the dissolution rate of abiotic control was 2.63 ± 0.3 × 10^{-15} mol/cm^2/s. Comparison with

other studies also shows that our value is similar to those measured by others, especially when differences in pH are taken into account. For example, Valsami-Jones et al. (1998) investigated the dissolution of apatite in the presence of aqueous metal cations over a range of pH with batch reactor experiments. They measured a dissolution rate of natural fluorapatite of 1.83×10^{-14} mol/cm^2/s in 0.1 mol/L $NaNO_3$ at pH 5.2. Welch et al. (2002) studied the effect of micro-organisms and microbial metabolites on apatite dissolution using batch reactors. In the abiotic experiments, the dissolution rate of fluorapatite was found to be 5×10^{-15} mol/cm^2/s in 1 mM NaCl at pH 5.5. Guidry and Mackenzie (2003) investigated fluorapatite dissolution using both a fluidized bed and stirred tank reactor over a range of pH. In 0.1 mol/L NaCl at a pH 6.5 and 5.9, they calculated the dissolution rate of 3.98×10^{-15} and 6.31×10^{-15} mol/cm^2/s.

It has been suggested that microbes can enhance mineral dissolution rates by producing organic ligands which can complex with metal ions to weaken the metal-oxygen bond to the mineral surface (Welch et al., 2002). Welch et al. (2002) found that the micro-organisms released pyruvate, acetate, lactate, propionate, formate and butyrate in the biological experiments with apatite. With regard to fungi, Hamdali et al. (2010) showed that peak P release coincided with a peak in the production of organic compounds that absorbed light at specific wavelengths, although the identity of these compounds was not reported. Microbes can also affect mineral dissolution reactions by uptake of phosphate from mineral surface or solution, thereby lowering solution saturation state in microenvironments surrounding the cells (Taunton et al., 2000).

Our data shows that apatite dissolution rates increased by 14% and 61% in the presence of *B. megaterium* and *P. agglomerans*, respectively. Thus, whereas the actual

401 rate values are within the variability for abiotic dissolution of apatite in the literature,
402 the percentage change is significant and above error, particularly for *P. agglomerans*.
403 Nevertheless, Hutchens et al. (2006) reported that microbes could inhibit mineral
404 dissolution through microbial colonization on mineral surfaces, thereby shielding
405 reactive surface sites from dissolution. The other possibility is that the adsorption of
406 Ca by bacteria underestimates the real dissolution rates (see section 3.5). In their
407 metal adsorption experiments using *Bacillus subtilis* cells, Yee et al. (2004) showed
408 that up to 65% of total Ca can be adsorbed to cell surfaces at pH 6.2, depending on the
409 ionic strength of the medium.
410
411 **3.4. Dissolved REE distribution patterns**
412
413 Since the apatite structure may accommodate relatively high concentrations of trace
414 elements, including REE, Sr, Y, Mn, U and Th, we analysed REE concentrations in
415 the aqueous phase in order to assess their release rates as a model of contaminant
416 metal mobilisation in general. The dissolved REE concentrations were normalized to
417 REE concentrations of FAP determined in our laboratory, which were used to reveal
418 the effects of chemical processes on the mobilization of REE. Similar
419 FAP-normalized dissolved REE patterns are observed in biotic and abiotic reactors
420 (Fig. 3). The patterns display higher heavy rare earth elements (HREE) relative to
421 light rare earth elements (LREE) and strong positive Eu anomalies. This implies that
422 HREE and Eu are released from FAP more easily than LREE and middle rare earth
423 elements (MREE). Fluorapatite is enriched in LREE and MREE compared to HREE,
424 which suggests that FAP has a strong affinity to retain LREE and MREE in its crystal
425 structure. There is an inverse relation between the partition coefficient of the REE in

426 the mineral and the patterns of the REE release ratios (Shibata et al., 2006). The
427 overall FAP-normalized REE contents show a positive Eu anomaly because of
428 preferential incorporation of Eu(II) in Durango apatite (Roeder et al., 1987). Due to its
429 higher solubility Eu(II) is more easily leached from minerals than the trivalent REE
430 (van der Weijden and van der Weijden, 1995) and the dissolved REE pattern changes
431 accordingly.
432 The extraction of REE is controlled by both intrinsic (crystal-chemical) and external
433 (solvent-chemical) factors. In the FAP structure, the LREE and MREE should
434 preferentially substitute into Ca2 site (sevenfold coordination), whereas the HREE
435 should selectively occupy the Ca1 site (ninefold coordination) (Fleet and Pan, 1995;
436 Pan and Fleet, 2002). The compatibility between LREE and MREE and the
437 stereochemical environment of Ca2 has been prompted by the combined effects of
438 substitution mechanisms, spatial accommodation, equalization of bond valence, and
439 crystal field contribution (Pan and Fleet, 2002). According to crystallographic
440 considerations, the cations in Ca1 site are easier to remove than those located in the
441 Ca2 site due to their relative coordination and interatomic distances (Chaïrat et al.,
442 2007). Thus, the HREE could preferentially be released from the FAP surface because
443 of their high incompatibility with the FAP mineral structure.
444 Nevertheless, it is possible that the higher normalised HREE release rate is due to the
445 fractionation resulting from the preferential precipitation of LREE phosphates (section
446 3.2 above). Indeed, reported REE(PO_4) solubility equilibrium products show that
447 solubility decreases between La and Ce or Pr and then increases between Ce or Pr and
448 Lu (Liu and Byrne, 1997), which would be consistent with the LREE being
449 preferentially precipitated from solution relative to HREE. This would also be
450 consistent with observations of Köhler et al. (2005) who suggested that secondary

rhabdophane enriched in LREE was formed during apatite dissolution.

In order to check which of these two mechanisms might be operative, we also calculated relative release rates of all REE to Ca in the reactors of FAP + Bm and the control reactors, which are shown in Fig. 4. For *P. agglomerans*, there was rapid release of REE to solution reaching maximum concentrations during the first day of the experiment but the REE concentrations in solution were constant in the FAP + Pa reactors afterwards so relative release ratios could not be calculated. The release rates of LREE and MREE were less than r_{Ca}, indicating the preferential retention of LREE and MREE from the solid phase. In contrast, the release ratios of HREE and Eu were greater than r_{Ca}, indicating the preferential release of HREE and Eu from the solid phase especially in the presence of *B. megaterium*. However, calculated mineral saturation indices using Visual Minteq 3.0 show that the solutions were supersaturated with respect to all REE(PO_4) (Fig. 5). The calculated saturation indices decrease with increasing atomic number, suggesting that preferential LREE precipitation is possible. It is therefore not possible to isolate the dominant mechanism for explaining the higher HREE release rates relative to those of the LREE.

Another mechanism possibly leading to higher HREE release rates is the formation of stronger solution complexes with dissolved carbonate (Lee and Byrne, 1993). However, our speciation calculations suggested that carbonate complexation is not significant in the reactors. Meanwhile, organic complexation (as might be possible in the biotic reactors due to organic matter produced during microbiological metabolism) can also lead to higher HREE concentrations relative to LREE in the fluid phase but only at low REE/DOC ratios (Marsac et al., 2010) since REE-organic stability constants display concave-up patterns at high REE/DOC ratios (Tang and Johannesson, 2003; Pouret and Martinez, 2009). In the absence of data on organic

matter concentration, the complexing effect of organic matter cannot be evaluated in the current study.

3.5. Accounting for sorption of elements to bacteria in dissolution reactions.

Since bacterial cells can sorb (adsorption and cellular assimilation) significant amounts of Ca (Yee et al., 2004) and REE (Ngwenya et al., 2010) from solution at the pH levels in our experiments, the interpretation of apatite dissolution rates is somewhat complicated for the biotic reactors, leading to the suggestion that bacteria may have a minimal effect on these processes. In our system the amount of elemental sorption on bacterial surfaces has been estimated as intracellular elemental concentrations for planktonic bacteria collected from biotic reactors on day 26 (Table 3). Higher intracellular element concentrations were observed in *B. megaterium* than in *P. agglomerans*. *Bacillus megaterium* is characterized by its large size (2.5 μm × 2.5 μm × 10μm), which accounts for its 100-fold higher volume compared to *P. agglomerans*, and resulted in large surface area with high reactive site density. Furthermore, as a Gram-positive bacterium, *B. megaterium* could be expected to have higher sorptive capacity for metals than the Gram-negative bacterium *P. agglomerans*, because Gram-positive bacterial cell surfaces carry a thicker layer of peptidoglycan, which carries most of the proton-active functional groups (Cox et al., 1999; Ngwenya et al., 2003). Compared with the chemical composition of cell biomass in the reactors without FAP and with FAP, *B. megaterium* shows the higher metal accumulation ability than *P. agglomerans* (Table 3). However, due to lower cell densities of *B. megaterium* in the reactors relative to *P. agglomerans* (Fig. 1), both reactors yielded similar intracellular elemental concentrations on a dry weight basis. The measured

values agreed well with the Ca and P uptake by *B. fungorum* after interaction with basalt and granite (Wu et al., 2007; Wu et al., 2008).

In order to determine the temporal evolution of elemental sorption by bacteria, the values of elemental uptake by bacteria were multiplied by the time evolution of cell densities (Fig. 1), corrected for sampling volume loss (Fig. 6). The addition of intracellular element concentration to dissolved element concentration was regarded as total concentrations of elements released from fluorapatite. The use of planktonic cell densities should yield underestimates because the fraction of cells attached to particle surfaces as biofilm is not accounted for (Wu et al., 2008). However, this underestimate is likely balanced by the fact that the cell densities in Fig. 1 are for live cells and do not account for dead cells revealed using LIVE/DEAD staining. The results show similar ratios of intracellular Ca concentrations relative to the total Ca (~16%) for *B. megaterium* and *P. agglomerans*. As might be expected, similar intracellular Ca concentrations imply that Ca adsorption is not strain-selective, which means that dissolved Ca concentration represents the relative degree of fluorapatite weathering. By contrast, the ratio of P sorbed to *P. agglomerans* relative to the total P (40%) was higher than that of *B. megaterium* (20%). More importantly, accounting for intracellular P in total P released elevates the P concentration in FAP + Pa reactors above the other treatments, consistent with the relative Ca concentrations among the three treatments. As a result, similar Ca:P ratios were observed in the FAP + Pa and FAP + Bm reactors, and both tended towards stoichiometric dissolution during the late stages of the experiment. The results also confirm our earlier inference that *P. agglomerans* cells accumulate intracellular phosphate, which they can use to grow under conditions of phosphate limitation.

Figure 6d also shows that REE distribution patterns for both biotic reactors were quite

similar to REE patterns in the abiotic control after the former were adjusted by intracellular lanthanides concentration. The REE scavenging patterns reflect the depletion of REE through their adsorption to cell surfaces. In the uncorrected data (Fig. 3), the LREE were strongly depleted in solution (78 - 96% in the FAP + Pa reactors and 63 - 79% in the FAP + Bm reactors) relative to MREE (53 - 70% in the FAP + Pa reactors and 30 - 59% in the FAP + Bm reactors) and HREE (26 - 52% in the FAP + Pa reactors and 25 - 41% in the FAP + Bm reactors). The scavenging effect was stronger in the reactors with *P. agglomerans* than with *B. megaterium* due to high cell densities of *P. agglomerans*.

The negatively charged peptidoglycan sheet in bacterial cell surface which contains binding sites such as carboxylate, amines and phosphate favours sorption of positively charged REE (Tourney et al., 2008; González et al., 2010; Ngwenya et al., 2010; Takahashi et al., 2010; Gorman-Lewis, 2011). Previous studies showed that more than 80% of the cation could be adsorbed to the biomass at circum-neutral to alkaline pH in short-term adsorption experiments (Ngwenya et al., 2009). However during long-term processes, organic matter excreted by bacterial cell lysis is capable of complexing metals in solution, thus competing with the cell surface for adsorbed metal (Ngwenya, 2007; Tourney et al., 2009), which could account for the low bacterial adsorption percent in the current study except for the adsorption of LREE. It has been suggested the order of REE adsorption onto deprotonated particle surface is LREE > MREE > HREE at neutral pH (Pourret et al., 2010) due to differences in polarizability (Laveuf and Cornu, 2009), whereas HREE have high affinity for organic ligands according to their stability constants (Lee and Byrne, 1993; Pourret and Martinez, 2009). Solution complexation increases the affinity of HREE for the solution phase (Byrne et al., 1996). The work of Takahashi et al. (2010) also found

551 that this effect of complex formation reduced the distribution coefficient of HREE
552 between bacteria and water but had little effect on LREE at circum-neutral pH. It is
553 consistent with the current study in that LREE were strongly depleted in solution by
554 the adsorptive scavenging of bacteria, especially Ce, which accounts for the negative
555 Ce anomaly in the FAP + Pa reactor.
556 The REE patterns reflect a combination of processes expected to occur in
557 bacteria-bearing systems, including fluorapatite weathering, reactions in solution,
558 bacterial uptake, and precipitation of secondary REE(PO_4) phases. As the REE(PO_4)
559 could be adsorbed to the cell wall through the formation of ternary surface complexes
560 (Ngwenya, 2007) or developed on cell surfaces through the effect of
561 bio-mineralization (Jiang et al., 2010), the amount of precipitated REE in the biotic
562 reactors is difficult to quantify.
563
564 **4. SUMMARY AND CONCLUSIONS**
565
566 This study demonstrated that the release of Ca and P in the biotic reactors with *P.*
567 *agglomerans* and *B. megaterium* was greater than those of the abiotic control. The
568 release rates in the biotic reactors increased above error compared with the abiotic
569 control, suggesting that these two bacteria increase apatite dissolution rates to some
570 degree. More importantly, the elevated dissolution rates in the presence of bacteria,
571 which occur in the early stages of bacterial growth lead to maintenance of higher
572 solution P concentrations throughout the duration of the experiment. The higher P
573 concentrations can thus be taken as evidence that the involvement of bacteria is likely
574 to lead to a higher eutrophication status of the soil porewaters and riverine waters.
575 Mass balance accounting for microbial uptake of metals and phosphate suggests that

some Ca and P released from apatite may be incorporated in the biomass. Our analysis may help to explain the ambiguous nature of the role of bacteria in this and previous mineral dissolution rate studies (Valsami-Jones et al., 1998; Guidry and Mackenzie, 2003; Köhler et al., 2005). Microbially-mediated REE release patterns reflect the complex interaction between the fluorapatite-bacteria surfaces and solution. The REE patterns suggested that the HREE were preferentially released from the mineral phase especially in the presence of bacteria, but that the LREE were retained on the solid phases including cell surfaces and/or by precipitation with phosphate. Microbially-mediated dissolution results suggest that microbe-fluorapatite interactions could play a role in the geochemical cycling of phosphate and trace metals in the aquatic environment.

*Acknowledgements.*This work was supported by International Foundation for Science (Grant Number: W/4502), the National Natural Science Foundation of China (Grant Number: 40603023) and Science and Technology Planning Project of Yunnan Province, China (Grant Number: 2009 CC025). M. Feng acknowledges the hospitality accorded by the School of GeoSciences during her stay in the University of Edinburgh. We thank Dr. A. N. Mariano for providing the Durango fluorapatite used in this study. Constructive reviews by two anonymous referees and the comments from the Associate Editor Roy A. Wogelius helped us to clarify our arguments.

598 **REFERENCES**

599

600 Byrne R. H., Liu X. and Schijf J. (1996) The influence of phosphate coprecipitation
601 on rare earth distributions in natural waters. *Geochim. Cosmochim. Acta* **60**,
602 3341-3346.

603 Chaïrat C., Schott J., Oelkers E. H., Lartigue J. E. and Harouiya N. (2007) Kinetics
604 and mechanism of natural fluorapatite dissolution at 25C and pH from 3 to 12.
605 *Geochim. Cosmochim. Acta* **71**, 5901-5912.

606 Chatli A. S., Beri V. and Sidhu B. S. (2008) Isolation and characterisation of the
607 phosphate solubilising microorganisms from the cold desert habitat of Salix Alab
608 Linn in trans Himalayan region of Himachal Pradesh. *Indian J. Microbiol.* **48**,
609 267-273.

610 Cox J. S., Smith D. S., Warren L. A. and Ferris F. G. (1999) Characterising
611 heterogeneous bacterial surface functional groups using discrete affinity spectra
612 for proton binding. *Environ. Sci. Technol.* **33**, 4514-4521.

613 Feng M. H., Pan J. Z., Ke F. and Li W. C. (2008) Water pollution of post-mined lands
614 in Lake Fuxian watershed in Yunnan Province. *J. Lake Sci. (In chinese)* **20**,
615 766-772.

616 Fleet M. E. and Pan Y. M. (1995) Site preference of rare earth elements in fluorapatite.
617 *Am. Mineral.* **80**, 329-335.

618 Golterman H. L. (1973) Natural phosphate sources in relation to phosphate budgets: a
619 contribution to the understanding of eutrophication. *Water Res.* **7**, 3-17.

620 González A. G., Shirokova L. S., Pokrovsky O. S., Emnova E. E., Martínez R. E.,
621 Santana-Casiano J. M., González-Dávila M. and Pokrovski G. S. (2010)
622 Adsorption of copper on Pseudomonas aureofaciens: Protective role of surface

623 exopolysaccharides. *J. Colloid Interf. Sci.* **350,** 305–314.
624 Gorman-Lewis D. (2010). Enthalpies of proton adsorption onto Bacillus licheniformis
625 at 25, 37, 50, and 75C. *Geochim. Cosmochim. Acta* **75**, 1297–1307.
626 Govindaraju K. (1984) Compilation of working values and sample description for 170
627 International References samples on mainly silicate rocks and minerals.
628 *Geostandard Newslett. Special vol. VIII* **1**, 8.
629 Guidry M. W. and Mackenzie F. T. (2003) Experimental study of igneous and
630 sedimentary apatite dissolution: control of pH, distance from equilibrium, and
631 temperature on dissolution rates. *Geochim. Cosmochim. Acta* **67**, 2949-2963.
632 Hamdali H., Smirnov A., Esnault C., Ouhdouch Y. and Virolle M. J. (2010)
633 Physiological studies and comparative analysis of rock phosphate solubilization
634 abilities of Actinomycetales originating from Moroccan phosphate mines and of
635 Streptomyces lividans. *Appl. Soil Ecol.* **44**, 24–31.
636 Harris N. J., New P. B. and Martin P. M. (2006) Laboratory tests can predict beneficial
637 effects of phosphate-solubilising bacteria on plants. *Soil Biol. Biochem.* **38**,
638 1521-1526.
639 Hutchens E., Valsami-Jones E., Harouiya N., Chaïrat C., Oelkers E. H. and
640 McEldoney S. (2006) An experiment investigation of the effect of *Bacillus*
641 *Megaterium* on apatite dissolution. *Geomicrobiol. J.* **23**, 177-182.
642 Jiang M., Ohnuki T., Kozai N., Tanaka K., Suzuki Y., Sakamoto F., Kamiishi E. and
643 Utsunomiya S. (2010) Biological nano-mineralization of Ce phosphate by
644 *Saccharomyces cerevisiae*. *Chem. Geol.* **277**, 61-69.
645 Kang S. M., Joo G. J., Hamayun H., Na C. I., Shin D. H., Kim H. Y., Hong K. and Lee
646 I. J. (2009) Gibberellin production and phosphate solubilisation by newly isolated
647 strain of *Acinetobacter calcoaceticus* and its effects on plat growth. *Biotechnol.*

Lett. **31**, 277-281.

Köhler S. J., Harouiya N., Chaïrat C. and Oelkers E. H. (2005) Experimental studies of REE fractionation during water-mineral interactions: REE release rates during apatite dissolution from pH 2.8 to 9.2. *Chem. Geol.* **222**, 168-182.

Kuhl A. (1974) Phosphorus. In *Algal Physiology and Biochemistry* (eds. W. D. P. Stewart). Blackwell Scientific, Oxford, pp. 636–654.

Lasaga A. C. (1984) Chemical kinetics of water-rock interactions. *J. Geophys. Res.* **89(B6)**, 4009-4025.

Laveuf C. and Cornu S. (2009) A review on the potentiality of Rare Earth Elements to trace pedogenetic processes. *Geoderma* **154**, 1-12.

Lee J. H. and Byrne R. H. (1993) Complexation of trivalent rare earth elements (Ce, Eu, Gd, Tb, Yb) by carbonate ions. *Geochim. Cosmochim. Acta* **57**, 295-302.

Lee J. U. and Beveridge T. J. (2001) Interaction between iron and *Pseudomonas aeruginosa* biofilms attached to Sepharose surfaces. *Chem. Geol.* **166**, 193-202.

Li Y. X., Wang L., Qi Y. K. and Tang F. (2007) Studies on the phytoplankton development trend in Lake Fuxian, China. *J. Lake Sci. (in Chinese)* **19(2)**, 223-226.

Liu X. and Byrne R. H. (1997) Rare earth and yttrium phosphate solubilities in aqueous solution. *Geochim. Cosmochim. Acta* **61**, 1625-1633.

Marsac R., Davranche M., Gruau G. and Dia A. (2010). Metal loading effect on rare earth element binding to humic acid: Experimental and modelling evidence. *Geochim. Cosmochim. Acta*, **74**, 1749-1761.

Ng Kee Kwong K. F., Bholah A., Volcy L. and Pynee K. (2002) Nitrogen and phosphorus transport by surface runoff from a silty clay loam soil under sugarcane in the humid tropical environment of Mauritius. *Agric. Ecosys. Environ.* **91**,

673 147–157.
674 Ngwenya B. T., Sutherland I. W., Kennedy L. (2003) Comparison of the acid-base
675 behaviour and metal adsorption characteristics of a gram-negative bacterium with
676 other strains. *Appl. Geochem.* **18**, 527-538.
677 Ngwenya B. T. (2007) Enhanced adsorption of zinc is associated with aging and lysis
678 of bacterial cells in batch incubations. *Chemosphere* **67**, 1982-1992.
679 Ngwenya B. T., Mosselmans J. F. W., Magennis M., Atkinson K. D., Tourney J., Olive
680 V. and Ellam R. M. (2009) Macroscopic and spectroscopic analysis of lanthanide
681 adsorption to bacterial cells. *Geochim. Cosmochim. Acta* **73**, 3134-3147.
682 Ngwenya B. T., Magennis M., Olive V., Mosselmans J. F. W. and Ellam R. M. (2010)
683 Discrete site surface complexation constants for lanthanide adsorption to bacteria
684 as determined by experiments and linear free energy relationships. *Environ. Sci.*
685 *Technol.* **44**, 650-656.
686 Pan Y. M. and Fleet M. E. (2002) Compositions of the apatite-group minerals:
687 substitution mechanisms and controlling factors. In *Phosphates: geochemical,*
688 *geobiological, and materials importance.* (eds. M. J. Kohn, J. Rakovan, J. M.
689 Hughes). Mineralogical society of America, Reviews in mineralogy &
690 Geochemistry, **V 48**, pp. 427-448.
691 Pourret O., Gruau G., Dia A., Davranche M. and Molénat J. (2010) Colloidal control
692 on the distribution of rare earth elements in Shallow Groundwaters. *Aquat.*
693 *Geochem.* **16**, 31-59.
694 Pourret O. and Martinez R. E. (2009) Modeling lanthanide series binding sites on
695 humic acid. *J. Colloid Interf. Sci.* **330**, 45-50.
696 Powell N., Shilton A., Chisti Y. and Pratt S. (2009) Towards a luxury uptake process
697 via microalgae – Defining the polyphosphate dynamics. *Water Res.* **43(17)**,

4207-4213.

Roeder P. L., MacArthur D., Ma X. P., Palmer G. R. and Mariano A. N. (1987) Cathodoluminescence and microprobe study of rare-earth elements in apatite. *Am. Mineral.* **72**, 801-811.

Salvia-Castellví M., Iffly F. J., Borghtb P. V. and Hoffmanna L. (2005) Dissolved and particulate nutrient export from rural catchments: A case study from Luxembourg. *Sci. Total Environ.* **344**, 51-65.

Shibata S. N., Tanaka T. and Yamamoto K. (2006) Crystal structure control of the dissolution of rare earth elements in water-mineral interactions. *Geochem. J.* **40**, 437-446.

Takahashi Y., Yamamoto M., Yamamoto Y. and Tanaka K. (2010) EXAFS study on the cause of enrichment of heavy REEs on bacterial cell surfaces. *Geochim. Cosmochim. Acta* **19**, 5443-5462.

Tang J. and Johannesson K. H. (2003). Speciation of rare earth elements in natural terrestrial waters: assessing the role of dissolved organic matter from the modeling approach. *Geochim. Cosmochim. Acta*., **67**, 2321–2339.

Taunton A. E., Welch S. A. and Banfield J. F. (2000) Microbial controls on phosphate and lanthanide distributions during granite weathering and soil formation. *Chem. Geol.* **169**, 371-382.

Tourney J., Ngwenya B. T., Mosselmans, J. F. W. and Magennis M. (2009) Physical and chemical effects of extracellular polymers (EPS) on Zn adsorption to Bacillus licheniformis S-86. *J. Colloid Interf. Sci.* **337**, 381– 389.

Tourney J., Ngwenya B. T., Mosselmans J. W. F., Tetley L. and Cowie G. L. (2008) The effect of extracellular polymers (EPS) on the proton adsorption characteristics of the thermophile *Bacillus licheniformis S-86*. *Chem. Geol*. **247**, 1–15.

723 Valsami-Jones E., Ragnarsdottir K. V., Putnis A., Bosbach D., Kemp A. J. and Cressey
724 G. (1998) The dissolution of apatite in the presence of aqueous metal cations at pH
725 2-7. *Chem. Geol.* **151**, 215-233.
726 van der Weijden C. H. and van der Weijden R. D. (1995) Mobility of major, minor and
727 some redox-sensitive trace elements and rare-earth elements during weathering of
728 four granitoids in central Portugal. *Chem. Geol.* **125**, 149-167.
729 Welch S. A., Taunton A. E. and Banfield J. F. (2002) Effect of microorganisms and
730 microbial metabolites on apatite dissolution. *Geomicrobiol. J.* **19**, 343-367.
731 Wu L., Jacobson A. D., Chen H. C. and Hausner M. (2007) Characterization of
732 elemental release during microbe-basalt interactions at T = 28°C. *Geochim.*
733 *Cosmochim. Acta* **71**, 2224-2239.
734 Wu L., Jacobson A. D. and Hausner M. (2008) Characterisation of elemental release
735 during microbe-granite interactions at T = 28°C. *Geochim. Cosmochim. Acta* **72**,
736 1076-1095.
737 Wu L. M., Forsling W. and Schindler P. W. (1991) Surface complexation of calcium
738 minerals in aqueous solution: 1. surface protonation at fluorapatite-water
739 interfaces. *J. Colloid Interf. Sci.* **147**, 178-185.
740 Xie X., Yan M., Wang C., Li L. and Shen J. (1989) Geochemical standard reference
741 samples GSD 9–12, GSS 1–8 and GSR 1–6. *Geostandard. Newslett.* 13, 83-179.
742 Yee N., Fowle D. A. and Ferris F. G. (2004) A Donnan potential model for metal
743 sorption onto *Bacillus subtilis. Geochim. Cosmochim. Acta* **68**, 3657-3664.
744 Young E. J., Myers A. T., Munson E. L. and Conklin N. M. (1969) Mineralogy and
745 geochemistry of fluorapatite from Cerro de Mercado, Durango, Mexico. *U. S.*
746 *Geol. Sur. Prof. Paper* **650D**, D84-D93.
747 Zhao X. R., Lin Q. M. and Li B. G. (2002) The solubilization of four insoluble

748 phosphates by some microorganisms. *Acta Microbiol. Sinica (In Chinese)* **42**,
749 236-241.
750 Zhang S. Z., and Shan X. Q. (1997) The determination of rare earth elements in soil
751 by inductively coupled plasma mass spectrometry. *At. Spectrosc.* **18**, 140-144.

Table 1. Composition of the Durango fluorapatite as analysed in our laboratory.

Element	Concentration (mg/kg) (standard deviation given in parentheses)	Measured stoichiometry	Element concentration relative to Ca
P	188000 (3384)	6.1	0.62
Ca	392943 (7389)	9.8	1
La	3693 (186)	0.027	0.0027
Ce	4710 (3)	0.034	0.0034
Pr	423 (9)	0.0030	0.00031
Nd	1514 (92)	0.010	0.0011
Sm	189 (10)	0.0013	0.00013
Eu	17.8 (0.1)	0.00012	0.000012
Gd	170 (7)	0.0011	0.00011
Tb	22.8 (1.1)	0.00014	0.000015
Dy	120 (6)	0.00074	0.000075
Ho	23.9 (1.2)	0.00014	0.000015
Er	65.6 (3.3)	0.00039	0.000040
Tm	7.78 (0.4)	0.000046	0.0000047
Yb	42.4 (2.1)	0.00024	0.000025
Lu	5.04 (0.3)	0.000029	0.0000029
Fe	321 (11)	0.0057	0.00059
F	35310 (2016)	1.9	0.19
Cl	4150 (176)	0.12	0.012
As	790 (30)	0.011	0.0011

Table 2. Fluorapatite dissolution rates and elements concentrations at steady state in the reactors of fluorapatite with or without bacteria.

Experimental condition	Steady state concentration (μmol kg^{-1} solution)					$r_{Ca} \times 10^{-15}$ ($mol/cm^2/s$)
	Ca	P	La	Sm	Yb	
FAP	5179	1883	4.87	0.710	0.382	3.61 ± 0.10
FAP + Bm	5284	2637	4.23	0.630	0.363	4.11 ± 0.06
FAP + Pa	5961	2206	2.77	0.338	0.149	5.82 ± 0.35

.

Table 3. Chemical composition of cell biomass (Average ± range)

Reactor	La	Ce	Pr	Nd	Sm	Eu	Gd	Tb	Dy	Ho	Er	Tm	Yb	Lu	P	Ca
	10^{-16} µmol/cell														10^{-10}µmol/cell	
Pa	1.8±0.2	3.0±0.4	0.37±0.05	1.3±0.2	0.31±0.05	0.039±0.004	0.17±0.02	0.023±0.004	0.16±0.03	0.029±0.005	0.055±0.009	0.012±0.002	0.16±0.02	0.010±0.001	0.36±0.06	0.57±0.06
Bm	61.6±3.4	66.2±3.4	8.2±0.5	30.1±1.8	7.2±0.4	1.7±0.1	4.3±0.3	0.86±0.05	7.6±0.5	1.5±0.9	3.0±0.2	0.70±0.05	4.4±0.5	0.56±0.08	3.5±0.3	0.50±0.01
	10^{-14} µmol/cell														10^{-10}µmol/cell	
FAP + Pa	15.5±3.3	19.4±4.3	1.7±0.4	5.4±1.3	0.70±0.17	0.068±0.015	0.67±0.17	0.070±0.018	0.42±0.12	0.077±0.020	0.21±0.05	0.030±0.007	0.14±0.03	0.020±0.004	0.81±0.23	0.61±0.13
FAP + Bm	7756±346	9884±405	874±40	2758±129	359±15	35.4±1.2	350±19	38.5±1.9	224±12	42.1±2.0	114±5.7	15.2±1.0	84.0±8.0	11.3±1.4	202±13.6	332±3.4
	µg/g dry weight														g/g dry weight	
FAP + Pa	151±32	191±42	16.9±4.0	54.9±13.4	7.4±1.8	0.73±0.16	7.5±1.9	0.80±0.20	4.8±1.3	0.90±0.24	2.5±0.6	0.32±0.08	1.7±0.4	0.22±0.05	0.018±0.005	0.017±0.004
FAP + Bm	224±10	288±12	25.7±1.2	82.9±3.9	11.3±0.5	1.12±0.04	11.5±0.6	1.27±0.06	7.6±0.4	1.45±0.07	4.0±0.2	0.54±0.04	3.0±0.3	0.41±0.05	0.0013±0.001	0.028±0.001

,

Figures captions:

Fig. 1. Evolution of cell densities as a function of elapsed time in the biotic reactors with or without fluorapatite. Note that *Pantoea agglomerans* was able to grow in the absence of dissoluble phosphorus or apatite, suggesting that it may have accumulated phosphorus during growth in nutrient broth. Error bars indicate the standard deviation of triplicates

Fig. 2. Evolution of Ca (a), P (b), the ratios of Ca:P (c), and pH (d) as a function of elapsed time in the reactors of fluorapatite with or without bacteria. The solid horizontal line represents the chemically measured stoichiometric ratio of Ca:P (1.61) of the bulk Durango fluorapatite (Table 1). Error bars indicate the standard deviation of triplicates.

Fig. 3. REE distribution pattern in the reactors of fluorapatite with or without bacteria. Dissolved REE are normalized to the concentration of REE in apatite. Error bars indicate the variation of dissolved REE concentration during the whole experiment.

Fig. 4. The distribution pattern of the ratios of REE release rates relative to Ca release rates.

Fig. 5. The distribution patterns of saturation indices of $REE(PO_4)$ in the reactors of fluorapatite with or without bacteria.

Fig. 6. Evolution of theoretical (accounting for intracellular concentrations) Ca (a), P (b), ratios of Ca:P (c), and REE release ratios (d) as a function of time in the reactors of fluorapatite with or without bacteria. Note the similar ratios for the biotic reactors when intracellular concentrations are included in total Ca and P release from apatite. The solid horizontal line represents the chemically measured stoichiometric ratio of Ca:P (1.61) of the bulk Durango fluorapatite (Table 1). Error bars indicate the standard deviation of triplicates.

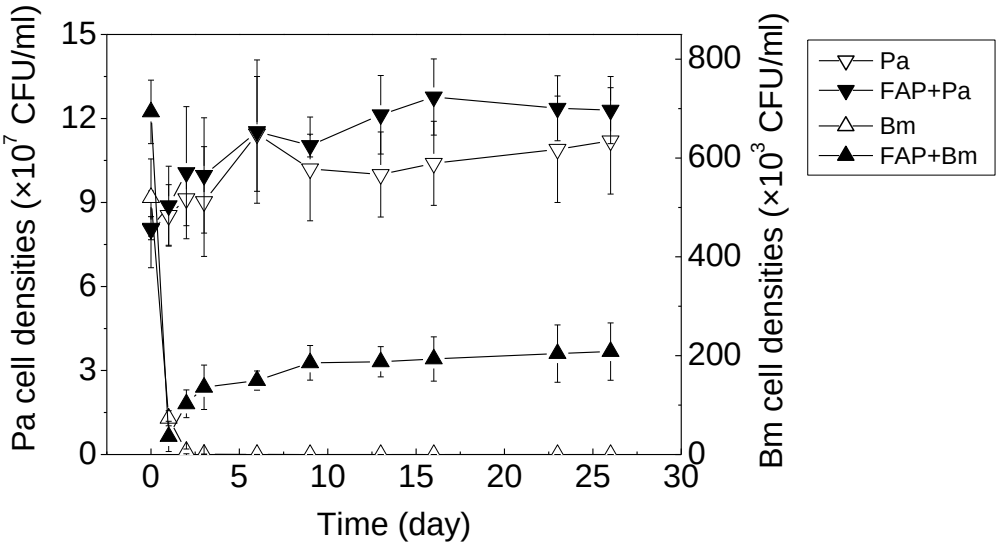
Pa cell densities (×10^7 CFU/ml)
Bm cell densities (×10^3 CFU/ml)
Time (day)
Pa
FAP+Pa
Bm
FAP+Bm
0
3
6
9
12
15
0
200
400
600
800
0
5
10
15
20
25
30

Fig. 1.

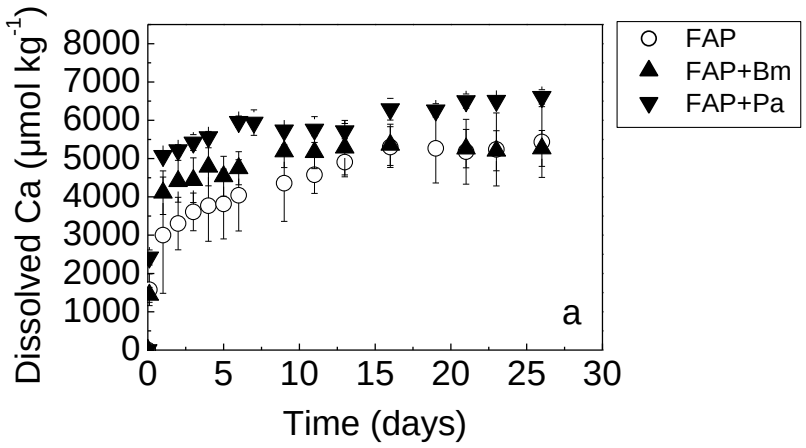
Dissolved Ca (µmol kg-1)
8000
7000
6000
5000
4000
3000
2000
1000
0
0
5
10
15
20
25
30
Time (days)
a
FAP
FAP+Bm
FAP+Pa

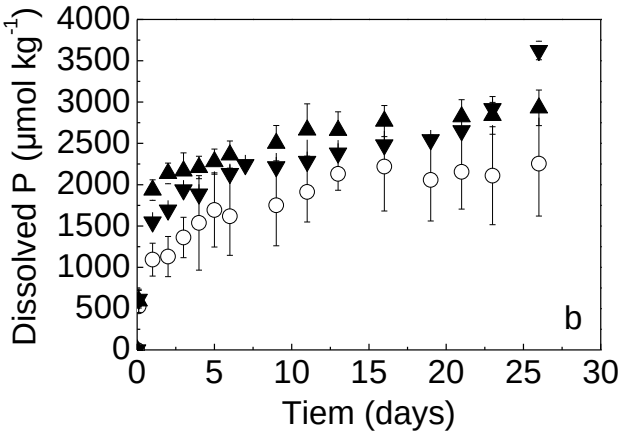
Dissolved P (µmol kg-1)
4000
3500
3000
2500
2000
1500
1000
500
0
0
5
10
15
20
25
30
Tiem (days)
b

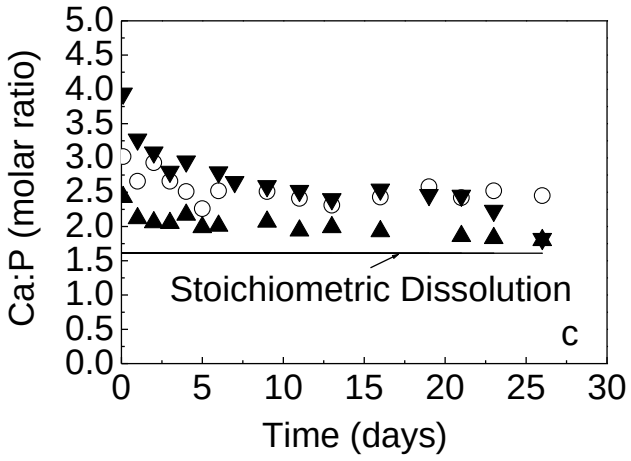
Ca:P (molar ratio)
5.0
4.5
4.0
3.5
3.0
2.5
2.0
1.5
1.0
0.5
0.0
0
5
10
15
20
25
30
Time (days)
Stoichiometric Dissolution
c

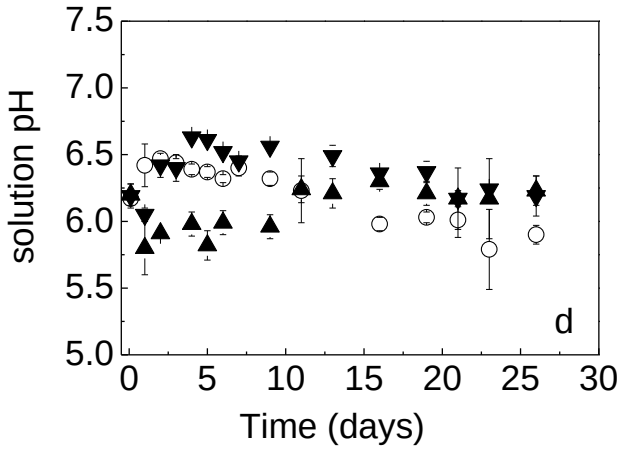

Fig. 2.

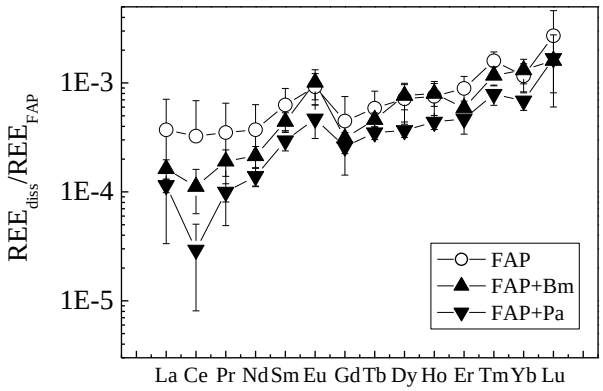
REE$_{diss}$/REE$_{FAP}$
1E-3
1E-4
1E-5
La Ce Pr Nd Sm Eu Gd Tb Dy Ho Er Tm Yb Lu
FAP
FAP+Bm
FAP+Pa

Fig. 3.

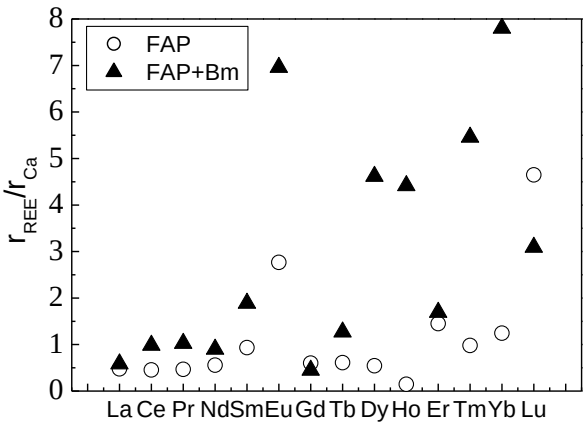
FAP
FAP+Bm
r_{REE}/r_{Ca}
0
1
2
3
4
5
6
7
8
La Ce Pr Nd Sm Eu Gd Tb Dy Ho Er Tm Yb Lu

Fig. 4.

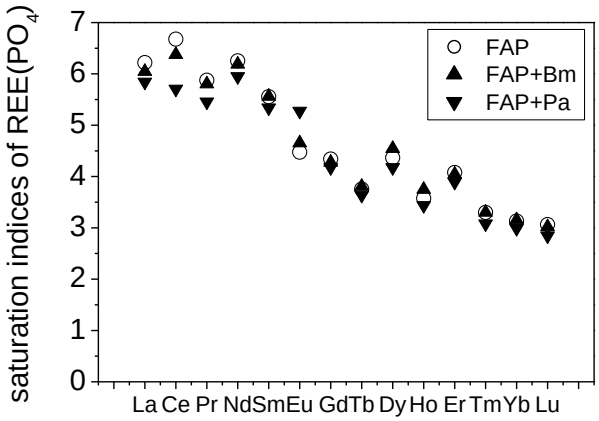
saturation indices of REE(PO4)
7
6
5
4
3
2
1
0
La Ce Pr Nd Sm Eu Gd Tb Dy Ho Er Tm Yb Lu
FAP
FAP+Bm
FAP+Pa

Fig. 5.

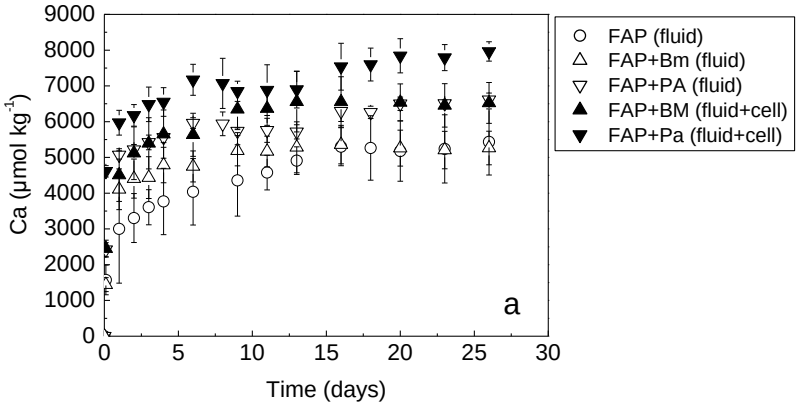
FAP (fluid)
FAP+Bm (fluid)
FAP+PA (fluid)
FAP+BM (fluid+cell)
FAP+Pa (fluid+cell)
Ca (µmol kg-1)
Time (days)
a

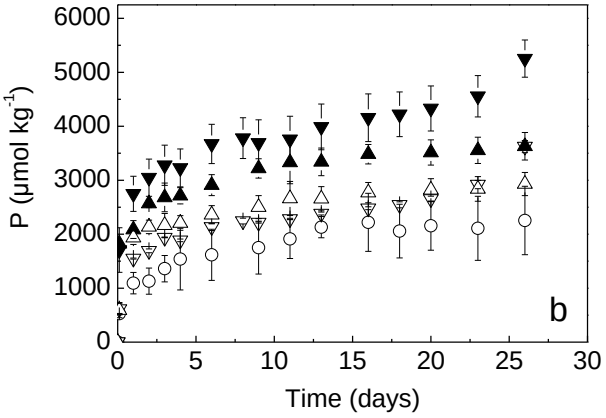
P (µmol kg-1)
Time (days)
b

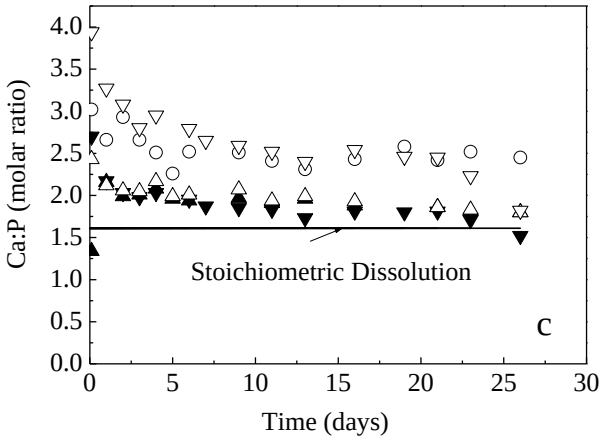
Ca:P (molar ratio)
Stoichiometric Dissolution
Time (days)
c

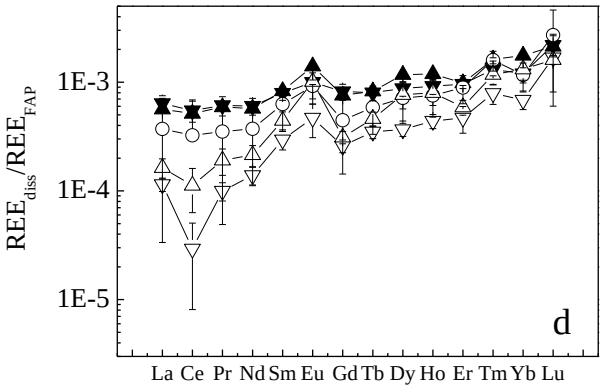
REE$_{diss}$/REE$_{FAP}$
1E-3
1E-4
1E-5
d
La Ce Pr Nd Sm Eu Gd Tb Dy Ho Er Tm Yb Lu

Fig. 6.

Figure(s)

Click here to download high resolution image

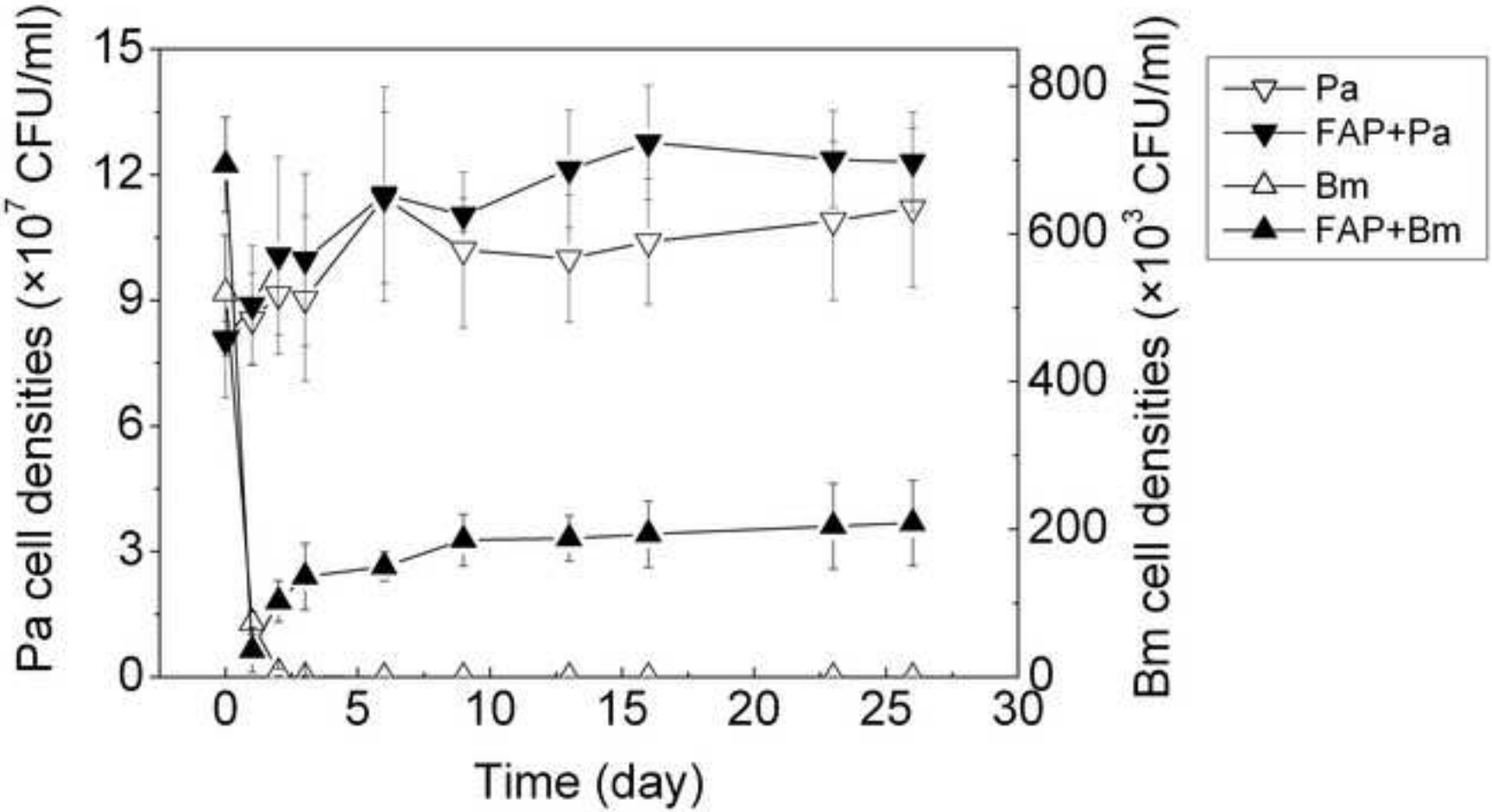

Fig. 1.

Figure(s)
Click here to download high resolution image

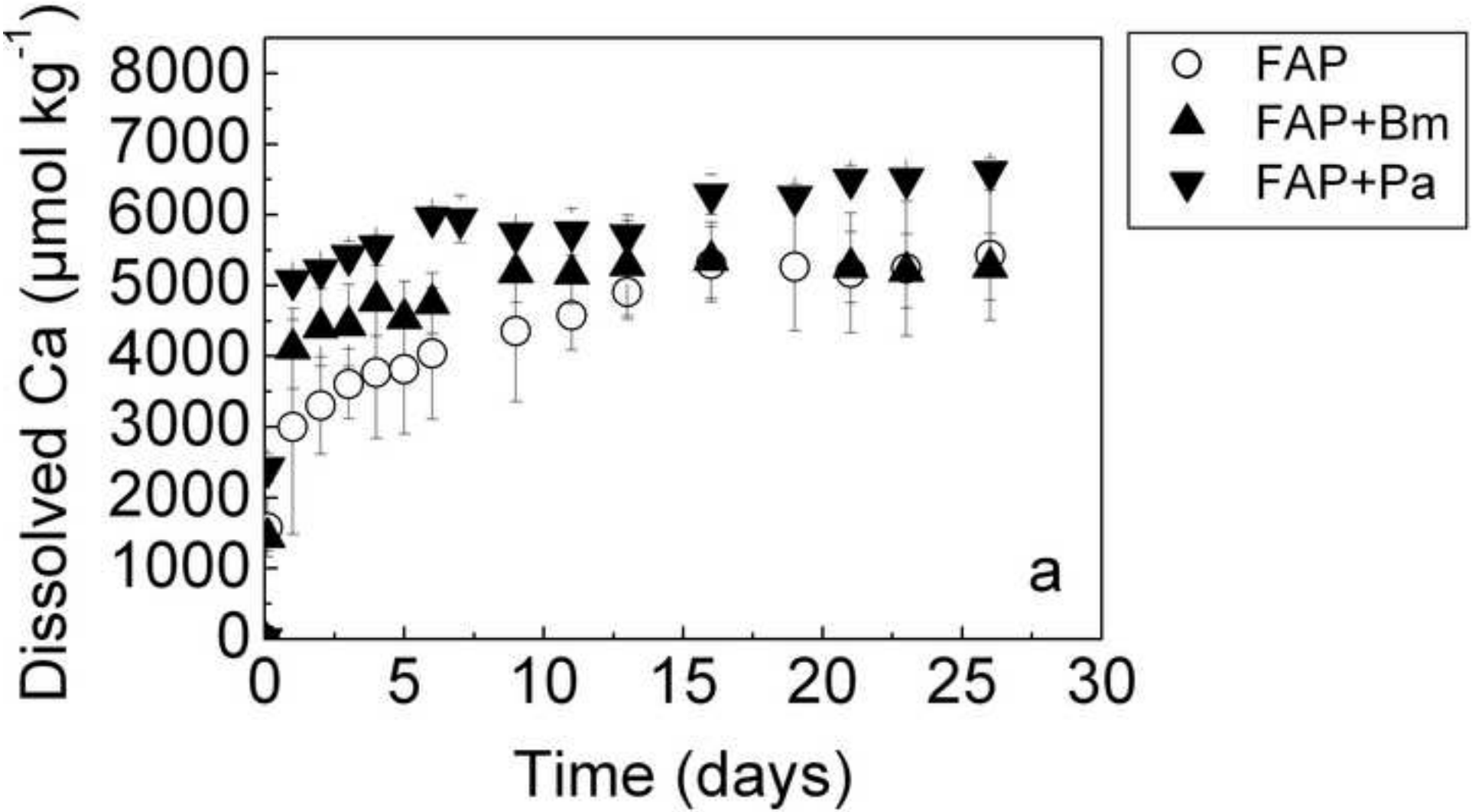

Fig. 2.

Figure(s)
Click here to download high resolution image

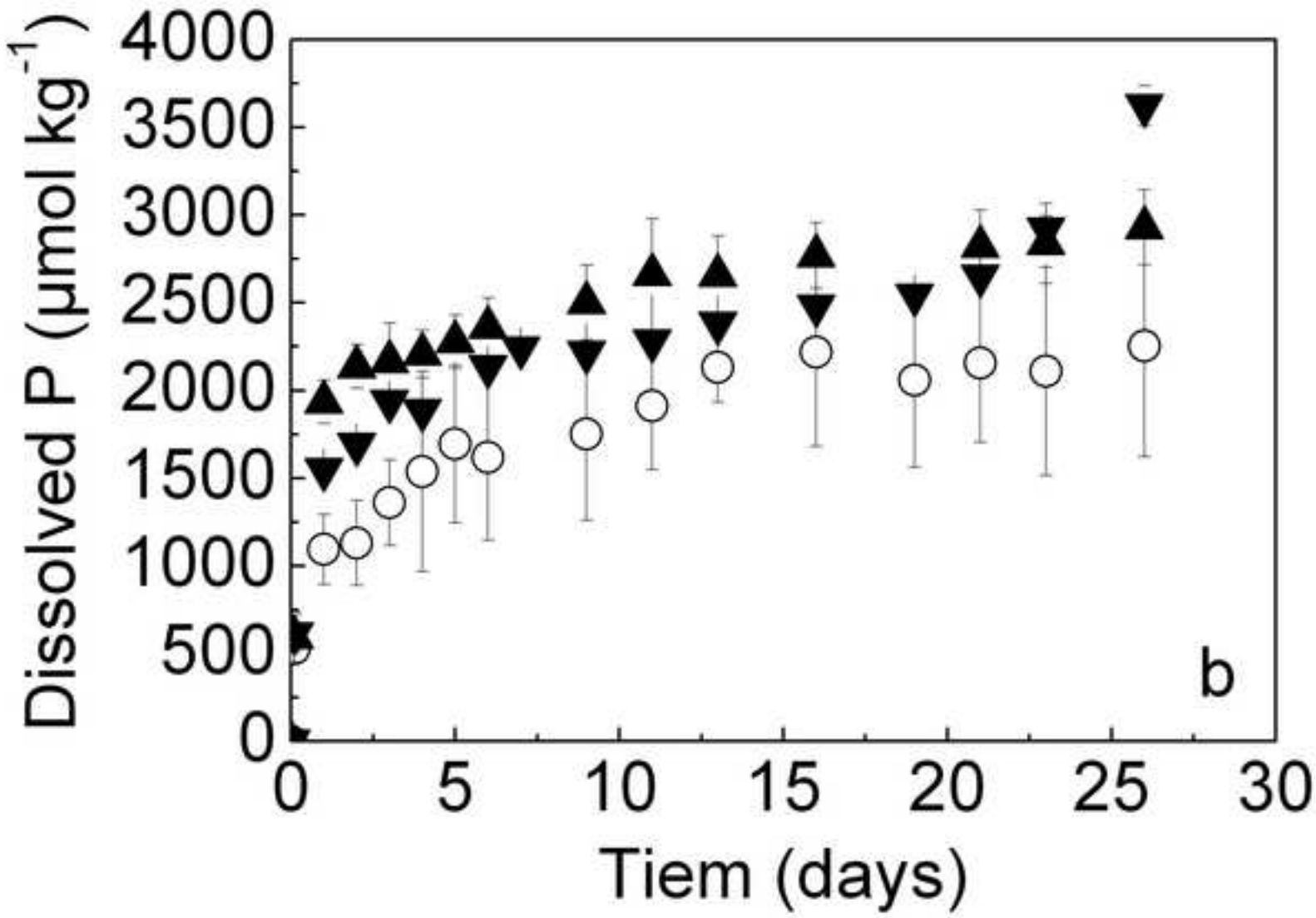

Fig. 2.

Figure(s)

Click here to download high resolution image

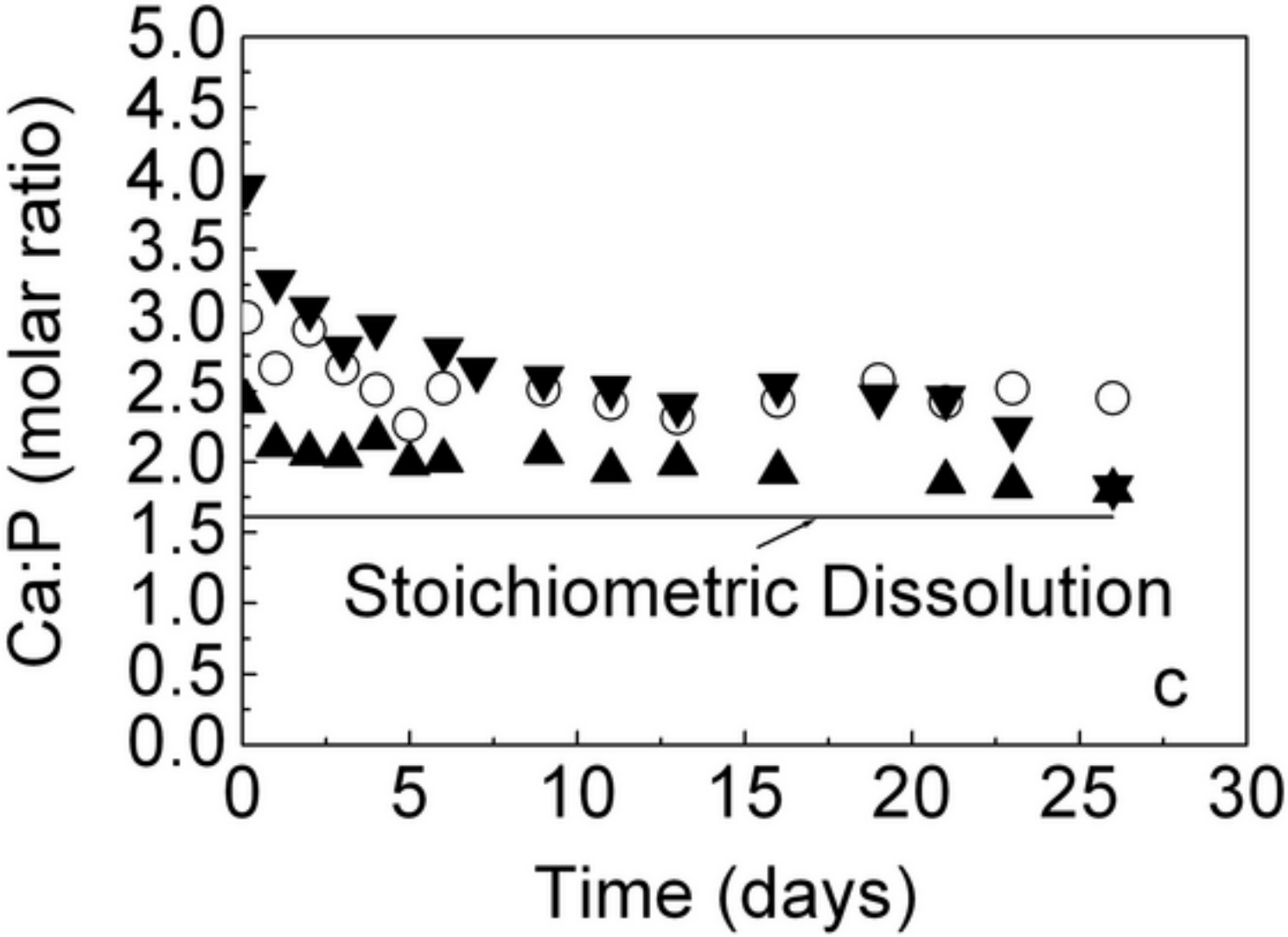

Fig. 2.

Figure(s)
Click here to download high resolution image

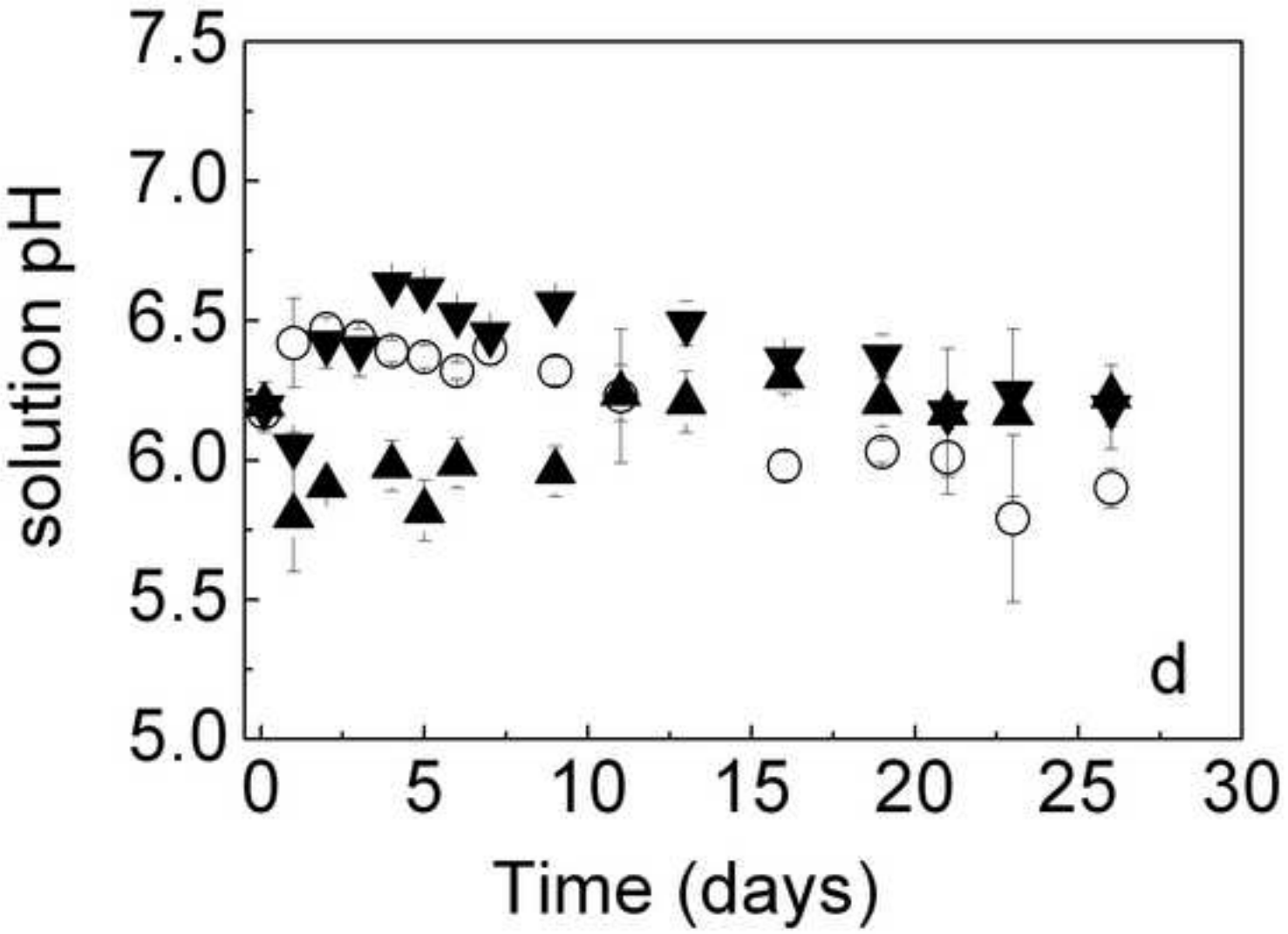

Fig. 2.

Figure(s)
Click here to download high resolution image

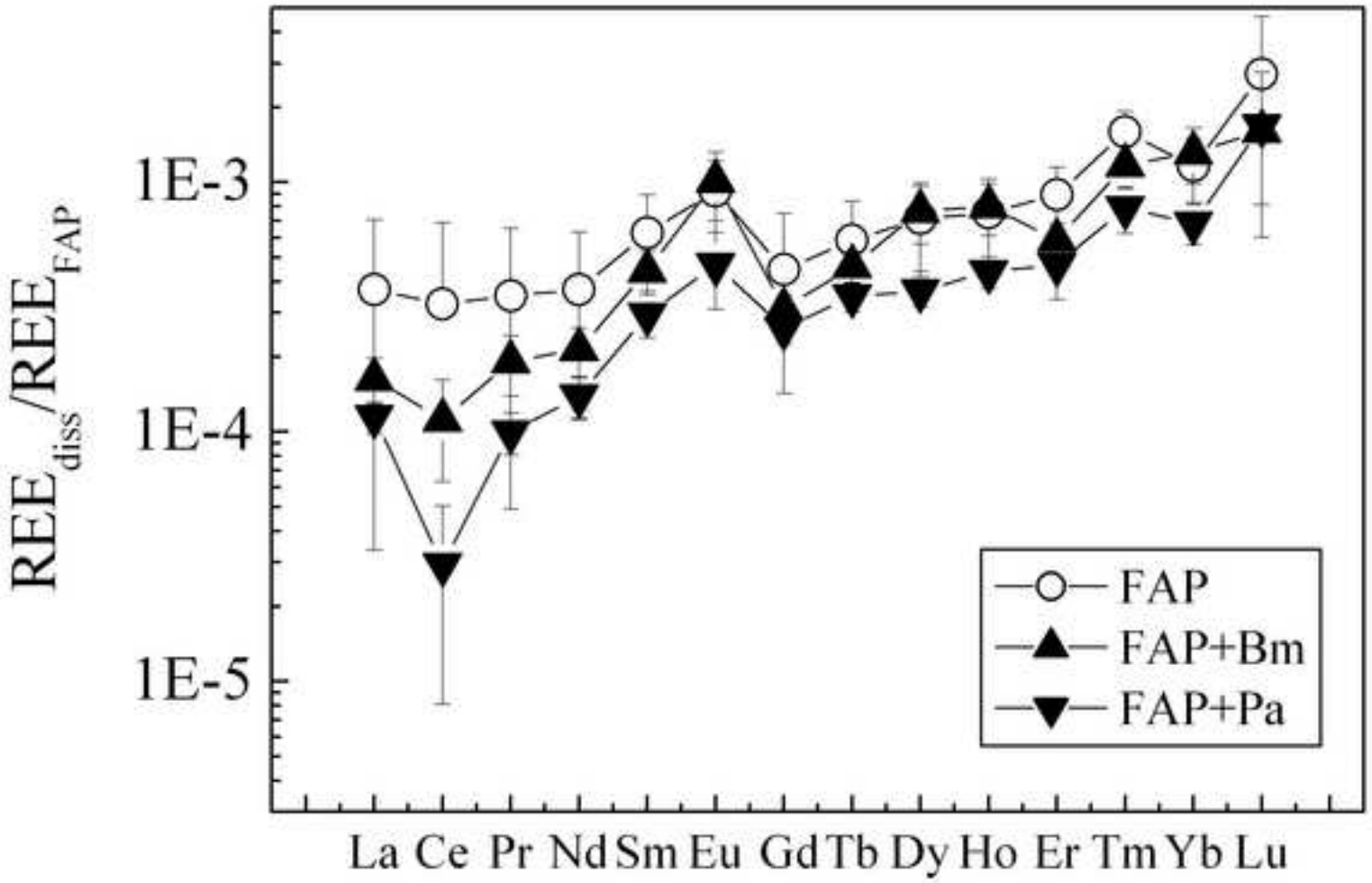

Fig. 3.

Figure(s)
Click here to download high resolution image

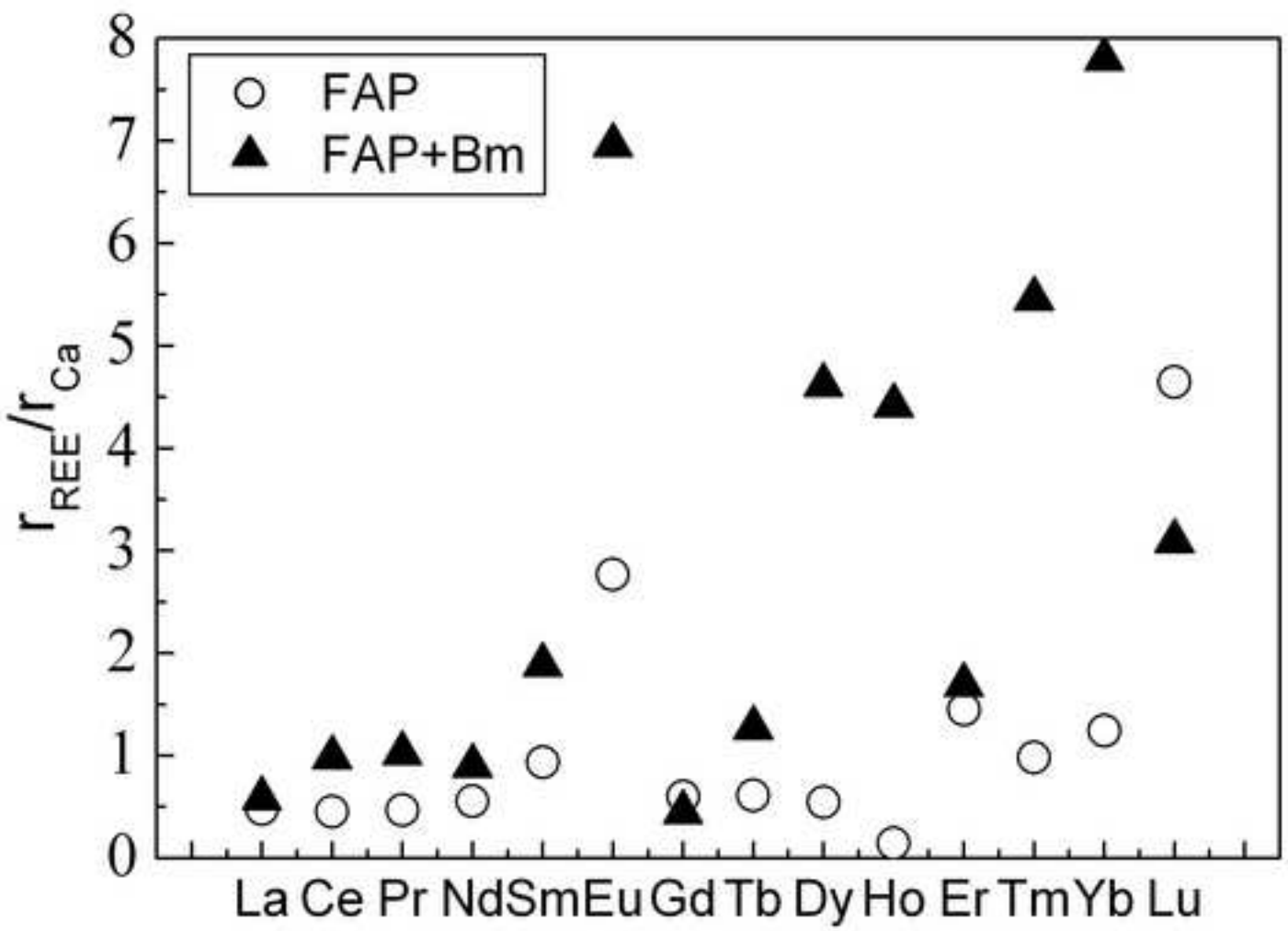

Fig. 4.

Figure(s)
Click here to download high resolution image

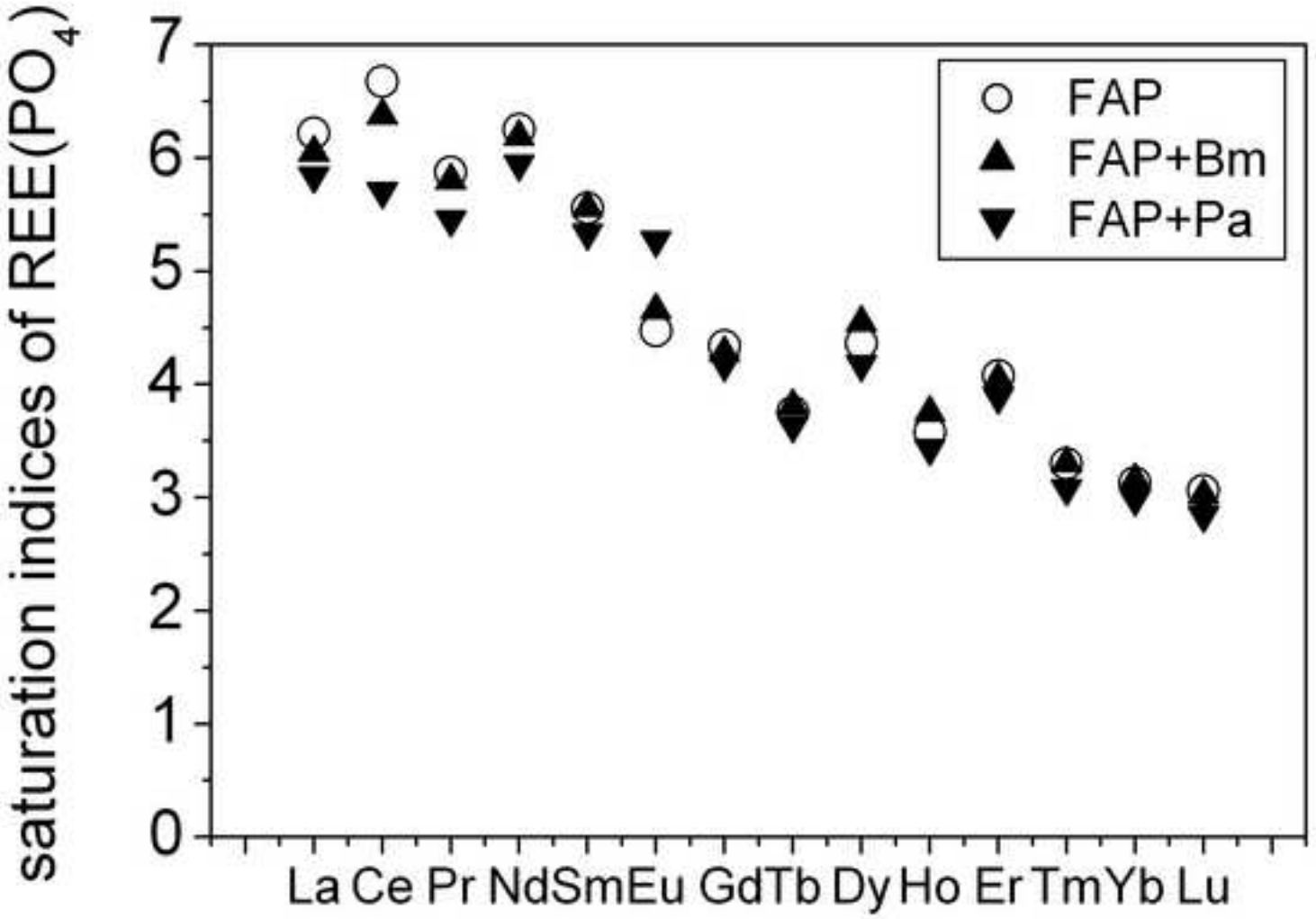

Fig. 5.

Figure(s)
Click here to download high resolution image

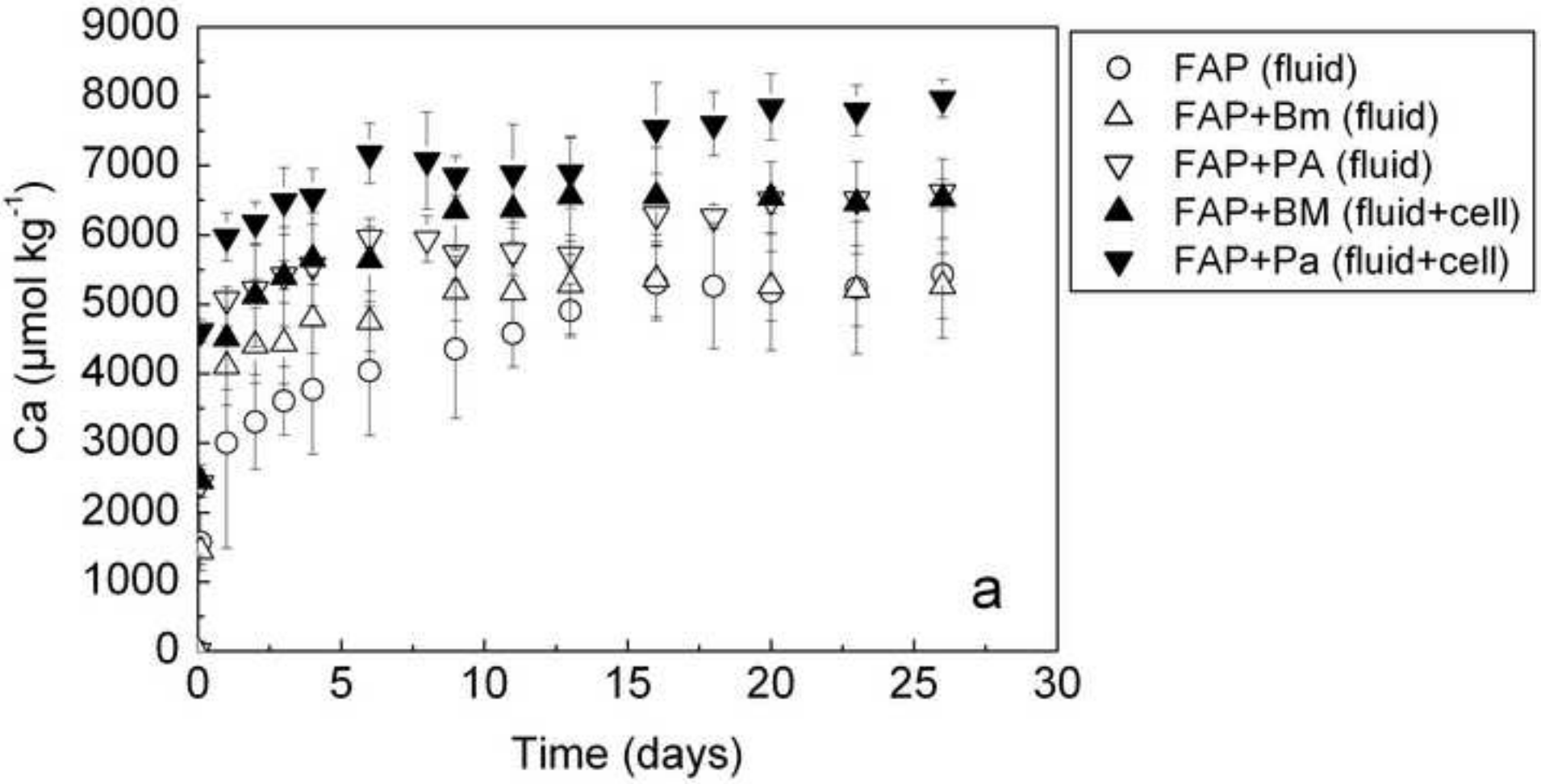

Fig. 6.

Figure(s)
Click here to download high resolution image

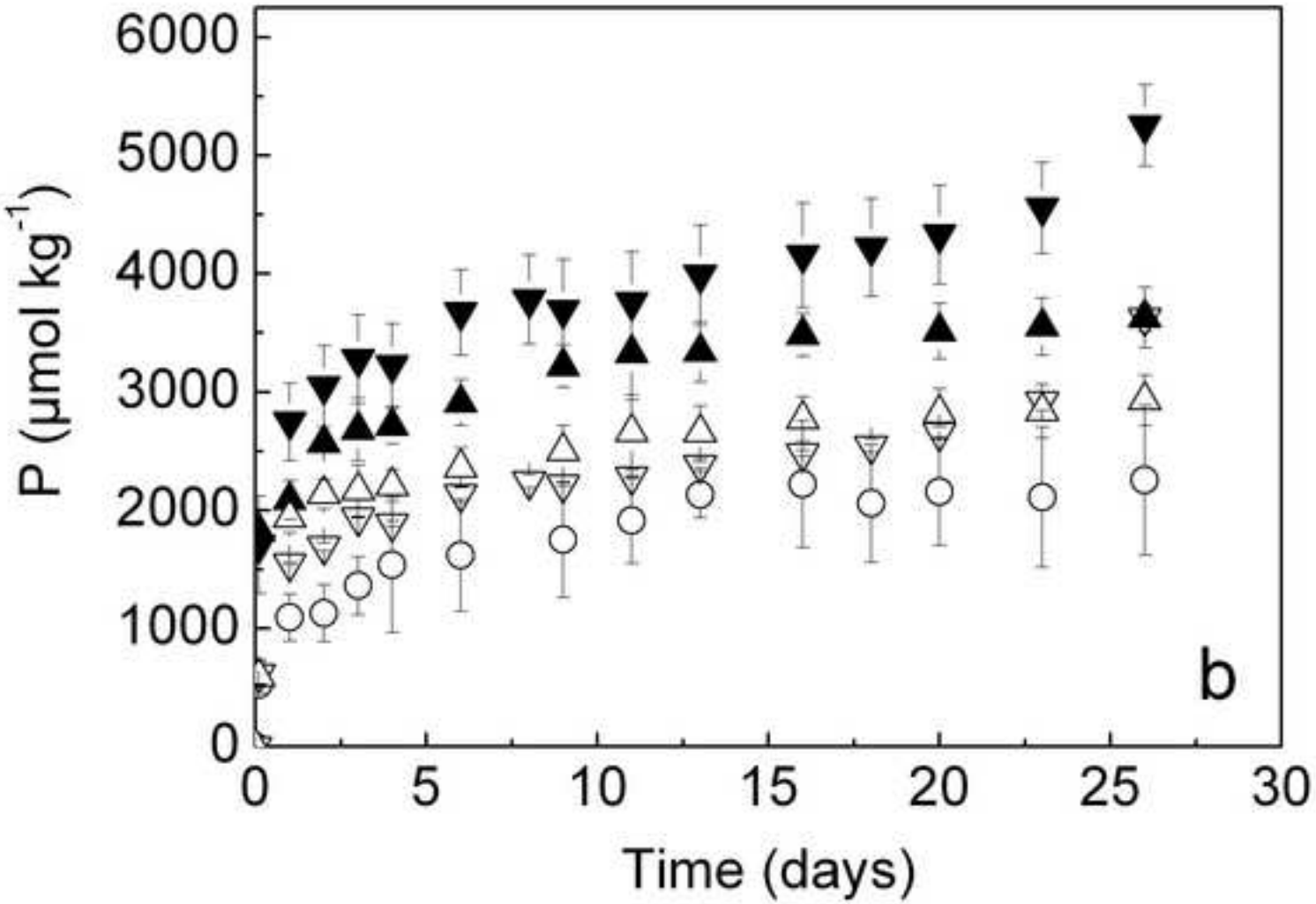

Fig. 6.

Figure(s)
Click here to download high resolution image

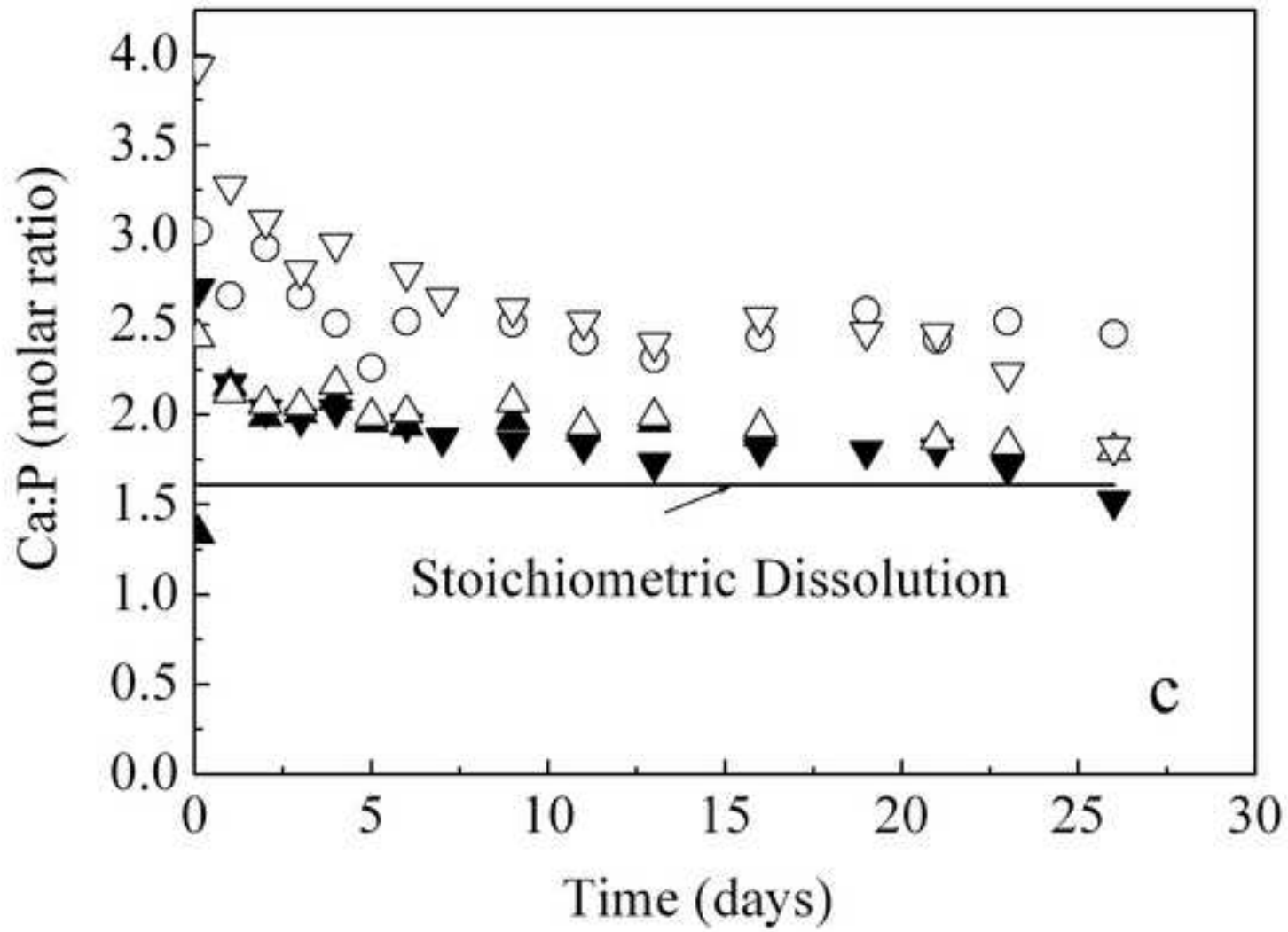

Fig. 6.

Figure(s)
Click here to download high resolution image

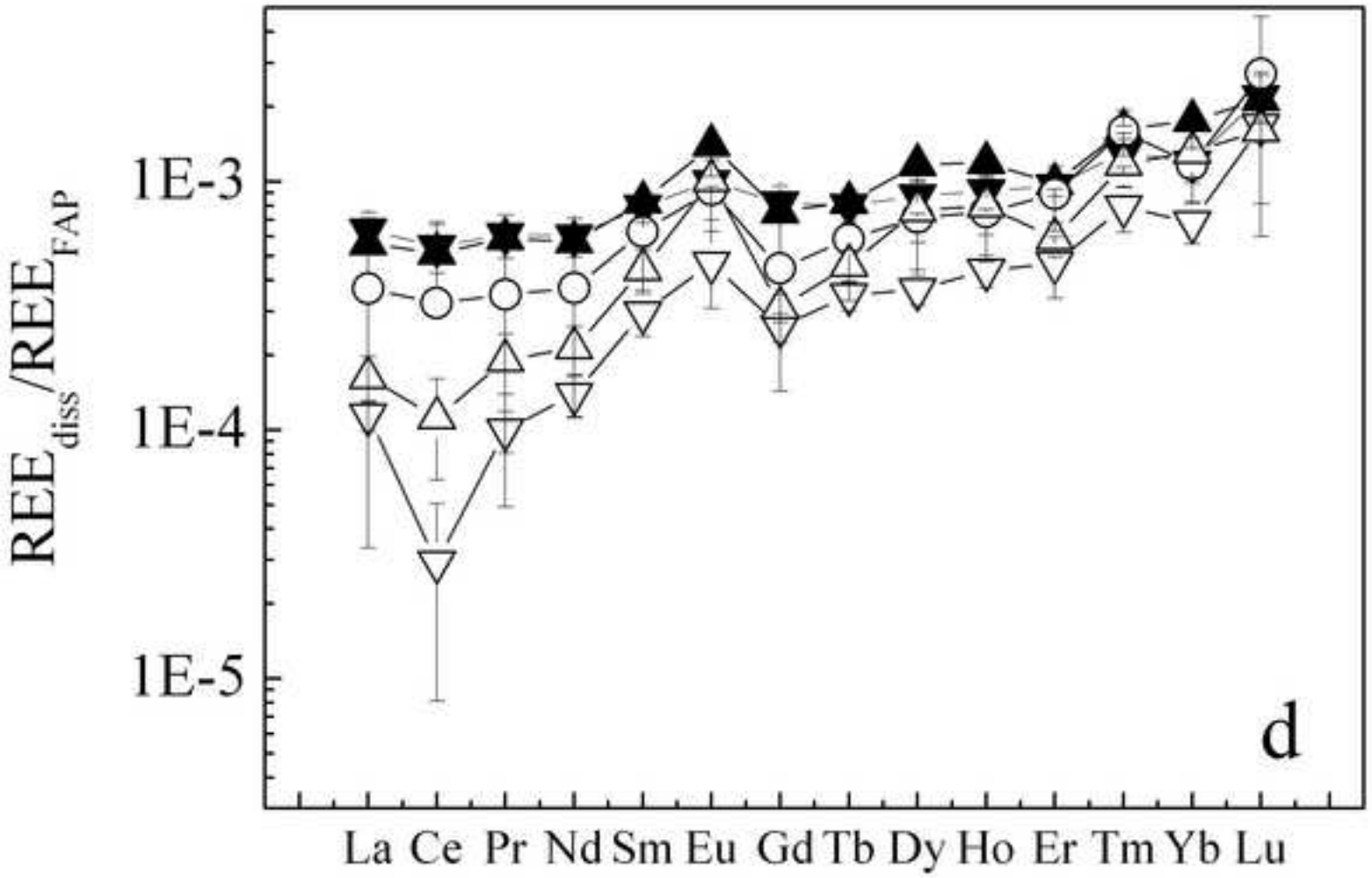

Fig. 6.

Figures captions:

Fig. 1. Evolution of cell densities as a function of elapsed time in the biotic reactors with or without fluorapatite. Note that *Pantoea agglomerans* was able to grow in the absence of dissoluble phosphorus or apatite, suggesting that it may have accumulated phosphorus during growth in nutrient broth. Error bars indicate the standard deviation of triplicates

Fig. 2. Evolution of Ca (a), P (b), the ratios of Ca:P (c), and pH (d) as a function of elapsed time in the reactors of fluorapatite with or without bacteria. The solid horizontal line represents the chemically measured stoichiometric ratio of Ca:P (1.61) of the bulk Durango fluorapatite (Table 1). Error bars indicate the standard deviation of triplicates.

Fig. 3. REE distribution pattern in the reactors of fluorapatite with or without bacteria. Dissolved REE are normalized to the concentration of REE in apatite. Error bars indicate the variation of dissolved REE concentration during the whole experiment.

Fig. 4. The distribution pattern of the ratios of REE release rates relative to Ca release rates.

Fig. 5. The distribution patterns of saturation indices of $REE(PO_4)$ in the reactors of fluorapatite with or without bacteria.

Fig. 6. Evolution of theoretical (accounting for intracellular concentrations) Ca (a), P (b), ratios of Ca:P (c), and REE release ratios (d) as a function of time in the reactors of fluorapatite with or without bacteria. Note the similar ratios for the biotic reactors when intracellular concentrations are included in total Ca and P release from apatite. The solid horizontal line represents the chemically measured stoichiometric ratio of Ca:P (1.61) of the bulk Durango fluorapatite (Table 1). Error bars indicate the standard deviation of triplicates.

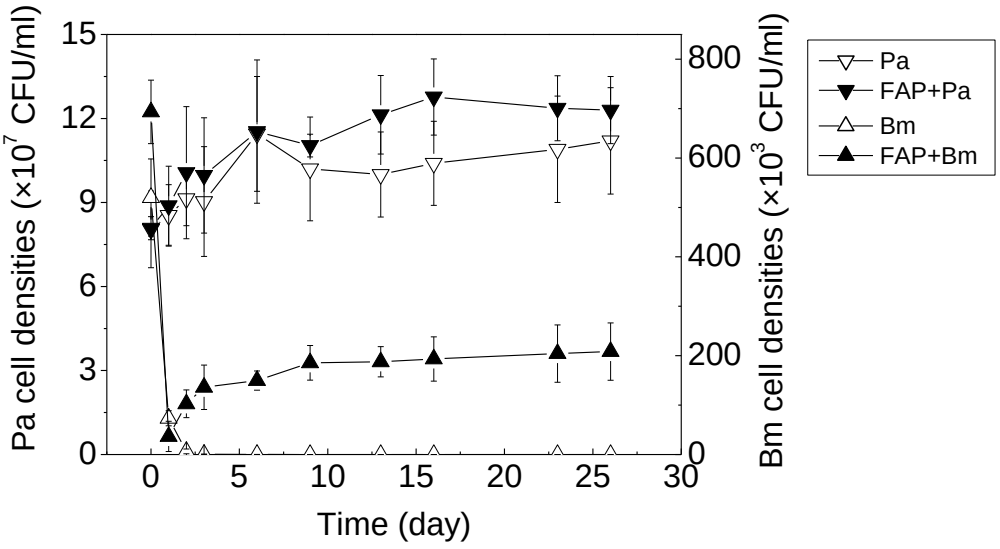
Pa cell densities (×10^7 CFU/ml)
Bm cell densities (×10^3 CFU/ml)
Time (day)
Pa
FAP+Pa
Bm
FAP+Bm
0
3
6
9
12
15
0
200
400
600
800
0
5
10
15
20
25
30

Fig. 1.

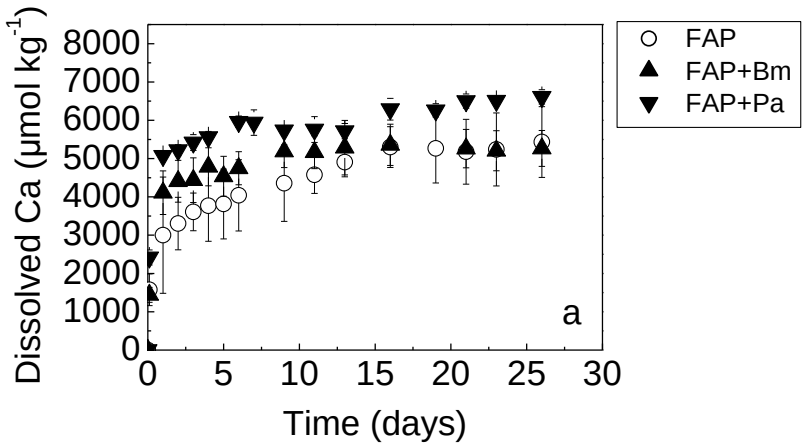
Dissolved Ca (µmol kg-1)
8000
7000
6000
5000
4000
3000
2000
1000
0
0
5
10
15
20
25
30
Time (days)
a
FAP
FAP+Bm
FAP+Pa

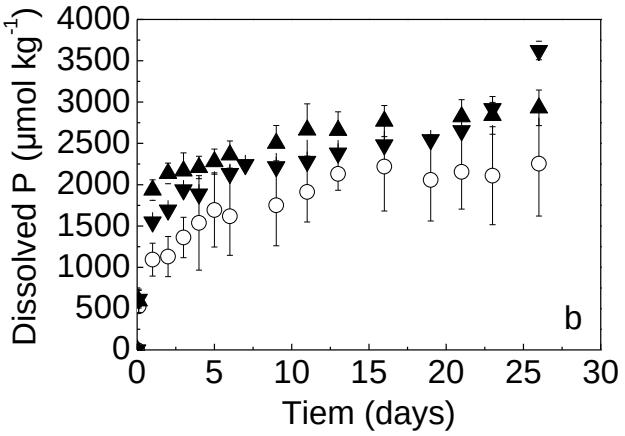
Dissolved P (µmol kg-1)
4000
3500
3000
2500
2000
1500
1000
500
0
0
5
10
15
20
25
30
Tiem (days)
b

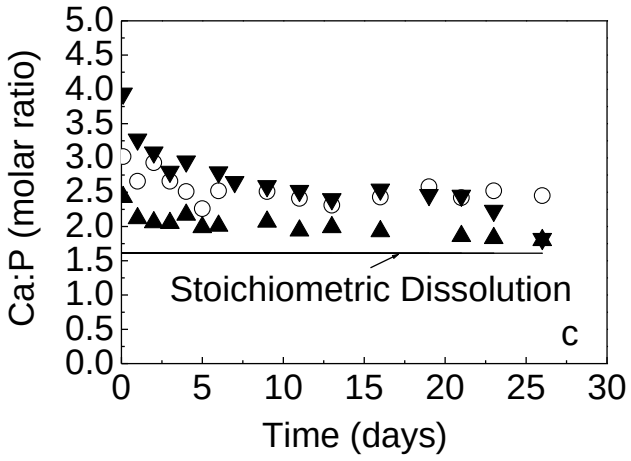
Ca:P (molar ratio)
5.0
4.5
4.0
3.5
3.0
2.5
2.0
1.5
1.0
0.5
0.0
0
5
10
15
20
25
30
Time (days)
Stoichiometric Dissolution
c

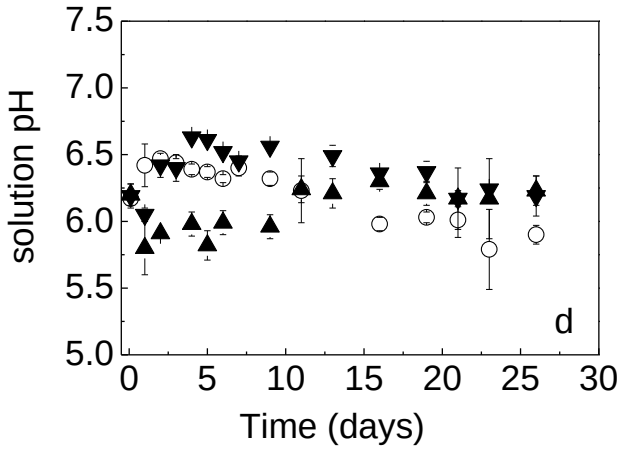

Fig. 2.

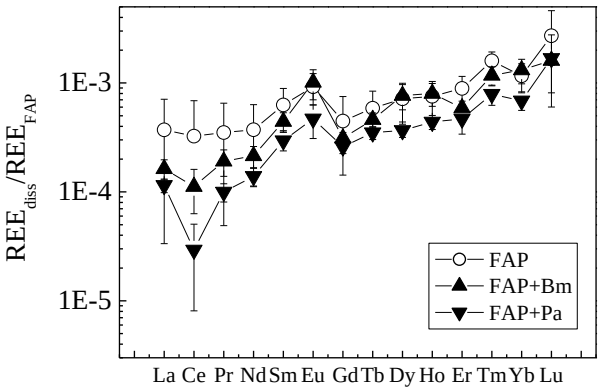
REE$_{diss}$/REE$_{FAP}$
1E-3
1E-4
1E-5
La Ce Pr Nd Sm Eu Gd Tb Dy Ho Er Tm Yb Lu
FAP
FAP+Bm
FAP+Pa

Fig. 3.

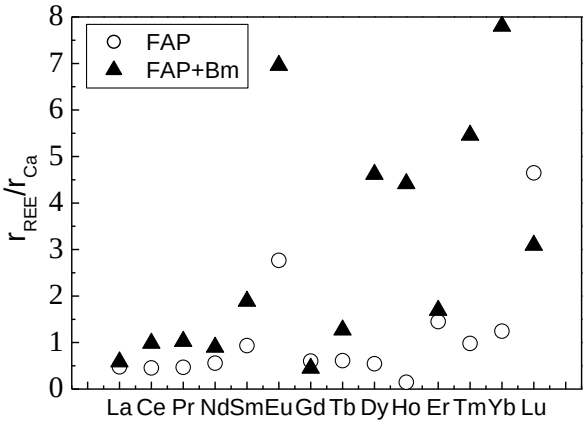
FAP
FAP+Bm
r_{REE}/r_{Ca}
0
1
2
3
4
5
6
7
8
La Ce Pr Nd Sm Eu Gd Tb Dy Ho Er Tm Yb Lu

Fig. 4.

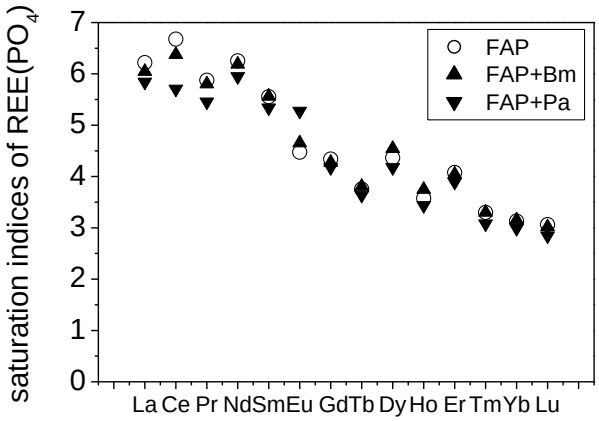
saturation indices of REE(PO4)
7
6
5
4
3
2
1
0
FAP
FAP+Bm
FAP+Pa
La Ce Pr Nd Sm Eu Gd Tb Dy Ho Er Tm Yb Lu

Fig. 5.

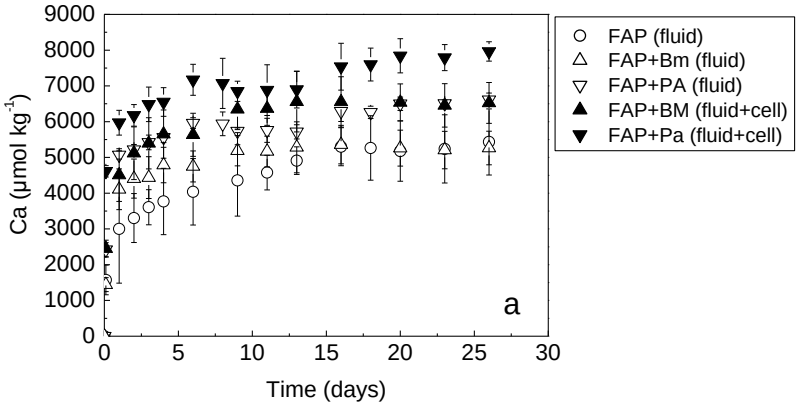
FAP (fluid)
FAP+Bm (fluid)
FAP+PA (fluid)
FAP+BM (fluid+cell)
FAP+Pa (fluid+cell)
Ca (μmol kg-1)
Time (days)
a

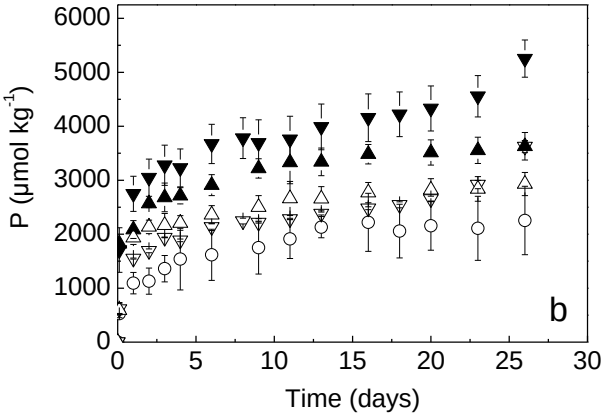
P (μmol kg-1)
Time (days)
b

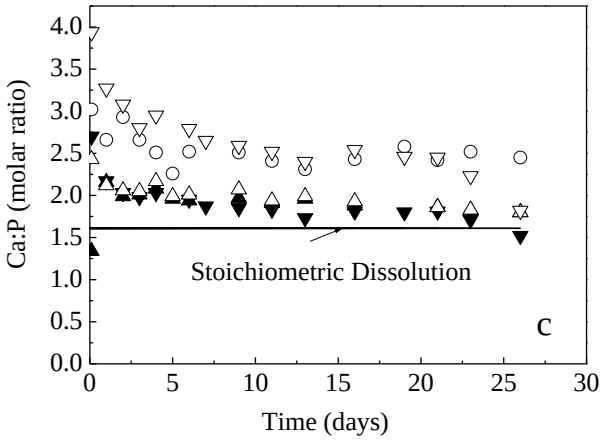
Ca:P (molar ratio)
Stoichiometric Dissolution
Time (days)
c

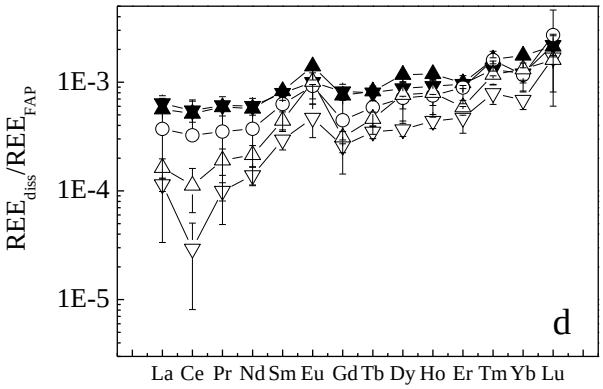
REE$_{diss}$/REE$_{FAP}$
1E-3
1E-4
1E-5
d
La Ce Pr Nd Sm Eu Gd Tb Dy Ho Er Tm Yb Lu

Fig. 6.